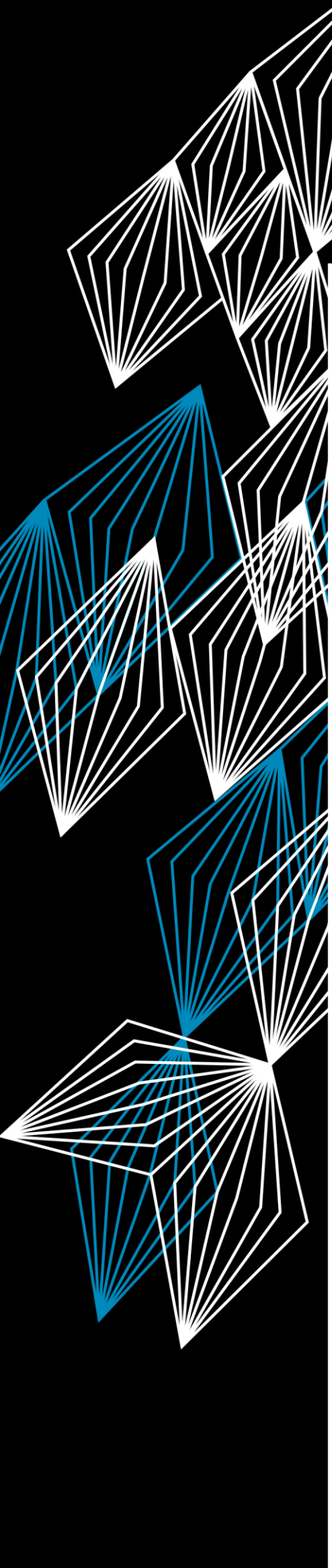

MASTER THESIS

Modeling Familial Hypertrophic Cardiomyopathy using Human Engineered Heart Tissues

T.R. van Iddekinge

Department of Applied Stem Cell Technologies (AST)
Faculty of Science & Technology
University of Twente, The Netherlands

Committee:
dr. M. Catarino Ribeiro (Daily supervisor)
prof. dr. P.C.J.J. Passier (Committee chair)
dr. ir. J. Rouwkema (External member)

08-07-2021

UNIVERSITY OF TWENTE.

Abstract

Familial hypertrophic cardiomyopathy (FHCM) is a prevalent and possibly fatal heart condition that strikes about 1 in 500 individuals. It can be caused by mutations in several genes, mutations in the MYBPC3 gene account for 20-25% of FHCM cases. These mutations can cause sarcomeric disarray and disorganization which can eventually cause hypertrophy of the intraventricular septum, defined as FHCM. As diagnosis and treatment of this condition remain a challenge, disease modeling of FHCM can give insight into the characteristics of the disease. It can give rise to new therapies and patient specific drug testing. human induced pluripotent stem cells (hiPSCs) are a good candidate for disease modeling. However, most disease models rely on 2D monolayer cultures that are generally immature and unable to efficiently recapitulate the contractile deficits present in a patient carrying the MYBPC3 mutation. A way to overcome these limitations is the use of 3D engineered heart tissues (EHTs). In this research, we developed an EHT disease model for FHCM using hIPSC derived cardiomyocytes (CMs), un-purified and lactate purified, with a CRISPR-CAS9 induced mutation in the MYBPC3 gene to understand the contractile parameters that are present in a patient carrying this mutation. We also attempted to develop an EHT based disease model treating healthy cells with hypertrophic stimulus phenylephrine (PE). We attempted to unveil a similar response in contraction force and velocity as in the MYBPC3 mutated disease model, due to the cells becoming hypertrophic. We found a significant decrease in contraction force and velocity between our control group and the mutated cell line, in experiments with and without lactate purified cells, more apparent than previous studies using 2D models, animal models, or 3D models. Stimulation with PE did not affect the contraction of our EHTs, thus having failed making a disease model with PE stimulation. Furthermore, we succeeded in making EHTs in a microfluidic chip co-cultured with endothelial cells (ECs), which is a very stable, reproducible and relatively easy method of EHT generation and can potentially be used in the future for making 3D hIPSC derived cardiac disease models, with the option of a constant medium perfusion making the EHT culture dynamic.

Abbreviations	
(c)EC	(cardiac) Endothelial cell
(c)FB	(cardiac) Fibroblast
CM	Cardiomyocyte
CRISPR	Clustered regularly interspaced short palindromic repeats
DMEM	Dulbecco's modified eagle medium
ECM	Extracellular matrix
EHT	Engineered heart tissue
FACS	Fluorescence-activated cell sorting
FHCM	Familial hypertrophic cardiomyopathy
GFP	Green Fluorescent Protein
HF	Heart failure
HS	Horse serum
KO/KI-Mice	Knock out/ Knock in mice
MYBPC(3)	Myosin Binding Protein 3
PE	Phenylephrine
TDI	T3 hormone, Dexamethasone, IGF
µEHT	micro Engineered heart tissue
VEGF	Vascular endothelial growth factor

Contents

1 Introduction and theoretical background

1.1 Familial Hypertrophic Cardiomyopathy (FHCM)

Familial Hypertrophic Cardiomyopathy (FHCM) is a genetic heart condition with a prevalence of around 1 in 500 individuals [1]. It is the most frequently occurring genetic heart condition in the United States. The main characteristic of the disease is thickening of the ventricular muscle wall of the heart, that separates the left and the right side of the ventricle. Figure 1 shows a schematic overview of the thickening of that ventricular wall. It is often paired with thickening of the left ventricular wall as can be seen in the figure. Other characteristics are myocyte disarray and sarcomere disorganization [1].

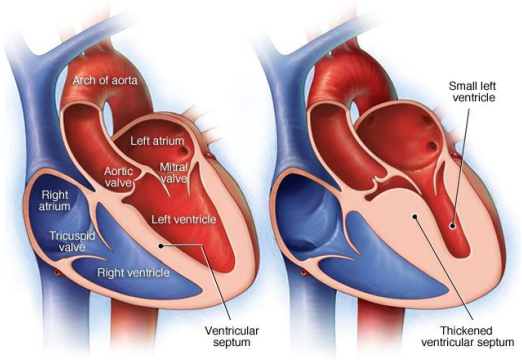

Figure 1: Schematic representation of the intraventricular septum of a patient with FHCM. Left: healthy heart. Right: Heart showing the characteristics of FHCM, with a thickened intraventricular septum and thickened wall of the left ventricle [2].

Symptoms of FHCM can vary per person and in the majority of cases, the progression and course of the disease are relatively benign. In many people, the disease goes undiagnosed and those people can lead relatively ordinary lives. However, FHCM is a major cause of heart failure (HF) and possibly sudden cardiac death (SCD) in adolescents and young adults, which makes a diagnosis urgent and makes it crucial to be able to detect the symptoms and give an accurate patient-specific treatment [3]. Other (less severe) symptoms of FHCM may include shortness of breath, chest pain, palpitations in the chest, lightheadedness, dizziness and often fainting.

FHCM may be of an obstructive or non-obstructive nature. When the left side of the ventricular septum is thickened, while not obstructing the blood flow inside of the left ventricle, we speak of non-obstructive FHCM [3]. The case may be that the septum is thickened so that it obstructs blood flow, which may cause leakage of blood back into the ventricle caused by obstruction of the mitral valve. In this case, we speak of obstructive HCM. A major problem with FHCM is that its onset may be late and has a late diagnostic cut-off point which may lead to underdiagnosis in many individuals [3].

1.2 Genetics of FHCM

FHCM has an autosomal dominant pattern of inheritance, meaning that only one mutated copy of the gene in each cell is needed to develop the disease, the expression and penetrance are variable [3]. Mutations in several genes can be the underlying cause of FHCM. The genes

most responsible for the development of the disease are MYH7, MYBPC3, TNNT2 and the TNNI genes [1, 3]. All these genes are responsible for synthesizing different proteins that play significant roles in forming structures in muscle cells that control the sarcomeric organization of cardiomyocytes (CMs). The two most commonly affected mutated genes are the MYH7 and the MYBPC3 gene, encoding for β-myosin heavy chain and myosin binding protein C (MyBPC) respectively [4]. The FHCM causing mutations associated with the MYH7 gene generally encode for missense mutations, which lead to incorporation of mutant type myosin in the sarcomere. Figure 2 shows the sarcomeric proteins that are associated with the disease progression of FHCM.

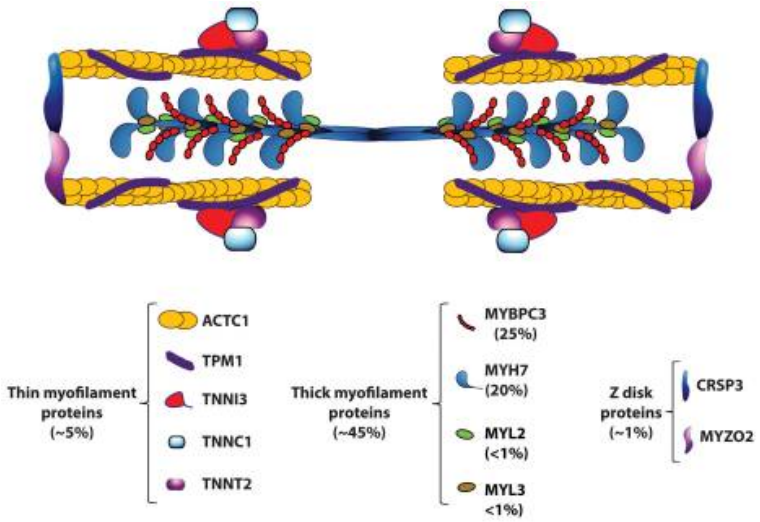

Figure 2: Proteins associated with the development of FHCM, as can be seen, the MYBPC3 disfunction accounts for the most cases of FHCM [3].

As stated above and can be seen in figure 2, the major protein defect is one in the MyBPC (+-30-35 % of all cases). In this project, we will focus on the MYBPC3 gene only. MyBPC is a component of the sarcomeric organization of the myocardium. In the mutated MYBPC3, the gene appears to produce C-terminally truncated proteins that lack binding sites for either myosin or actin. As a consequence, myocyte disarray and hypertrophy can occur, causing FHCM [5]. Van Dijk et al reported on the characterization of the underlying mutation causing FHCM. In the Netherlands, an estimated 35 % of FHCM patients have founder mutations in the MYBPC3 gene, with those founder mutations being c.2373dupG and c.2864-2865delCT as can be seen in figure 3 [6, 5].

Furthermore, the pathophysiology of FHCM is also influenced by impairment of the ubiquitin proteasome system (UPS), which is responsible for the degradation of proteins. This impairment gives rise to an increase in pro-hypertrophic and apoptotic factors, and the accumulation of misfolded proteins [7].

MyBPC has several roles in the biology of the cardiac sarcomeres, structural as well as functional. The protein is rod-shaped and can be found within the cardiac sarcomere [8]. It is bound to the myosin backbone with its C-terminal. The N-terminal of the protein powers muscle contractility and is bound to the actin or myosin filament.

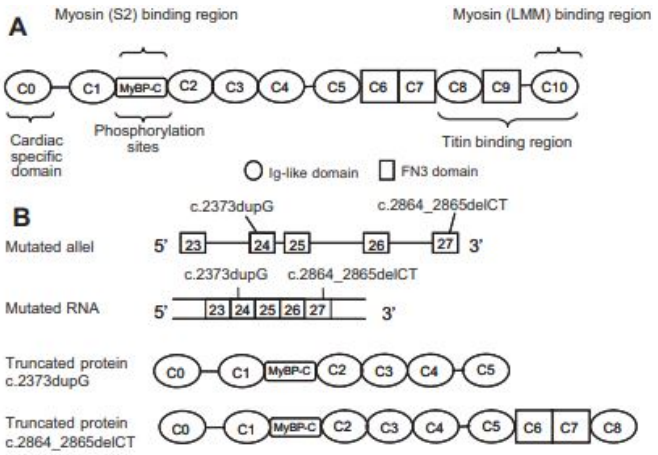

Figure 3: Schematic view of the founder mutations in the MYBPC3 gene associated with FHCM and the structure MYBPC3, consisting of 3 fibronectin domains and 8 immunoglobin domains. B shows the location of the founder mutations [5].

Previous research shows that the N terminals C0/C1 domains of the MyBPC3 interact with the actin and myosins S2 region using binding bases. This creates a sort of swinging mechanism that allows the MyBPC3 to switch between actin and myosin [7].

1.3 Pathogenesis of FHCM

The pathogenesis of FHCM involves many diverse mechanisms which determine the rate of development and the expression of the disease, and many patients are asymptomatic. FHCM can pathologically be seen as a four-step mechanism of disease development, where the first step logically is the genetic mutation, which is explained in the previous section of this report. Those mutations will induce intra-cellular changes to the DNA, and its effects will vary per mutation [3].

In response to the changes caused by the mutations, there will be molecular changes that change the function of the heart tissue. Several Ca2+ responsive processes (such as enhanced Ca2+ sensitivity of myofibrillar activity of ATPase and altered calmodulin-dependent protein kinase II activity [9]) and molecular pathways that play a crucial role in the programming of the hypertrophy of the heart are affected. By affecting these intermediary pathways, hypertrophic responses are arising, such as pressure overload-induced hypertrophy [3].
In response to the molecular changes, the clinical and histological phenotypes will start to occur, meaning the actual cardiac hypertrophy, ventricular fibrillation, fibrosis and heart failure (HF).

1.4 Diagnosis of FHCM

As can be seen in figure 1, the prominent clinical manifestation of FHCM is the thickening of the ventricular septum and left ventricular hypertrophy. The cut-off point for a diagnosis of FHCM is a ventricular septum thickness of more than 13mm at the end of the diastole. This thickness has to be accompanied by the absence of other secondary causes like hypertension or other pre-existing abnormalities, also pre-existing abnormal loading conditions have to be absent [3].

As those pre-existing conditions can be expressing within the course of FHCM development, it is tough to diagnose the disease and couple these conditions to the pathology of FHCM.

The most dangerous complication of FHCM is sudden cardiac death (SCD). A big risk group of FHCM associated SCD are professional athletes, so early diagnosis in this group is critical as professional adolescent athletes can also physiologically develop hypertrophy in the left ventricular septum due to their increased physical activities. This makes it hard to diagnose this group of patients because the pathological and physiological symptoms cannot be distinguished [3].

1.5 Treatment of FHCM

After patients are diagnosed with FHCM, they are evaluated through family history and a complete physical examination. As a pharmacological treatment, beta-adrenergic receptor blockers are the first viable option [3]. Other treatments include calcium channel blockers and heart rhythm drugs.

As most of the symptoms of FHCM are fairly mild, sudden cardiac death (SCD) is the most critical factor to be prevented in the disease development of FHCM. Therefore, disease management is crucial to prevent the risk of SCD. [3]

When the FHCM is really of an obstructive nature, surgery can be a treatment option. Typically, the required septal thickness to qualify for surgery is 15mm [10]. In highly symptomatic patients, removing a part of the intraventricular septum by surgery can restore the diastolic activity and can alleviate the symptoms that are related to the FHCM [10]. The blood-flow obstruction is often referred to as left ventricular outflow tract obstruction. The thickness of the hypertrophied ventricular septum is in 70% of the FHCM cases not enough to cause severe LVOTO [10]. However, in a portion of these patients, dormant obstruction can develop.

1.6 Models for studying heart disease

As FHCM is difficult to diagnose, can lead to HF, and is still poorly understood, there is a growing need for *in vitro* and *in vivo* disease models for understanding the complex underlying mechanisms of FHCM. These disease models can help understand the disease and lead to the development of potential treatments, as there is currently no cure or even an effective treatment available for FHCM [11]. A better understanding of the disease is therefore crucial. This subsection will cover some of the existing disease models for FHCM and their advantages and disadvantages, as it is still a great challenge to model FHCM effectively [12].

1.6.1 Animal models

In *vivo* animal models offer a valuable way of monitoring and studying different heart conditions [13]. However, there are many differences between the *in vivo* situation of animals and humans, as well in disease progression, development, and organ physiology [14, 15]. Also, humans and animals are exposed to different environmental stimuli. Therefore, the translation from the outcomes of studies in animal models to the actual human situation remains a challenge [13]. Various animal models of HCM have been used in the past for studying FHCM and the MYBPC3 mutation [16, 17, 18].

1.6.2 *In vitro* cardiac models, use of cell lines and primary cells

For decades, *in vitro* cardiac models have been used for disease modeling. An option for this is the use of primary cells, which are taken directly from the tissue of interest. As a consequence

of this, primary cells have an excellent representation of the *in vivo* state because they have not been modified and thus express their native phenotype. This is the reason that they have been studied and used for studying the toxic effects of drugs and normal biochemistry and physiology of cells [19], and the MYBPC3 mutation [5]. The variability of primary cells from different donors is an issue because the number of cells coming from one donor is limited, limiting the number of experiments that can be done with one primary cell batch. As primary cells are not genetically transformed, their lifespan and expansion capacity are very limited, and these cells are hard to maintain because they need specific growth factors and media [13]. Another disadvantage is that the collection of these cells often requires invasive procedures, as surgeons have to reach the tissue of interest. This is undoubtedly the case when harvesting primary cardiac cells, and therefore an unwanted side effect of studying patient-specific heart tissue. Primary CMs are being used extensively for research, but when kept in culture for a long time, they lose their morphology, cell count, and cell structure [20].

The vast majority of *in vitro* models rely on cell lines. Cell lines are easier to work with and generally more resistant and robust [19]. Cell lines can be seeded and re-cultured several times (called passages). They can be kept in culture for a long time, and many cells can be generated. A disadvantage of the use of these cell lines is that the properties of the cells can change during the number of passages they go through, this is called genetic drift [21]. Another major issue with the use of cell lines is misidentification. Examples of frequently used cardiac cell lines are the HL-1 [22] and the h9c2 [23] line. A few problems with CM cell lines is that they can be genetically unstable and have a significant variability between them, so it is hard to compare outcomes from different studies due to the variability between different used cell lines [24].

1.6.3 Stem Cells

Stem cells are widely used in research and can are divided into embryonic stem cells (ESCs), fetal stem cells, and adult stem cells. Stem cells are undifferentiated cells that have the potential to be differentiated into almost any cell type in the case of multi- and pluripotent stem cells. They differ in their potential to differentiate and proliferate [25]. ESCs are pluripotent and derived at an early stage of development (blastocyst stage). They can spontaneously differentiate into multiple germ layers and can be grown in culture. Adult stem cells are stem cells whose primary function is to repair the tissue they originate from. They are either unipotent or multipotent. Their differentiation potential is more limited than that of ESCs [26].

1.6.4 Human induced pluripotent stem cells (hiPSC)

Human induced pluripotent stem cells (hiPSCs) are adult somatic skin or blood cells that are reprogrammed using the Yamanaka factors (Oct4, Sox2, Klf4, c-Myc) [27, 28] to regain the ability to be differentiated into any alternative cell lineage. These reprogrammed cells have the growth properties and morphology of ESCs and express ESC genes [28]. This offers the opportunity for patient-specific disease and drug screening based on the cells that are collected from that particular patient and have their exact unique genotype [29, 27]. Thus, hiPSCs have got the capacity (under the right conditions) to differentiate into every other cell type. Therefore, they are a powerful tool to make patient-specific CMs, and with that are a good candidate for disease modeling of FHCM, which is also done in previous studies by studying FHCM utilizing a mutation in the MYBPC3 gene [8, 30, 31].

When patients carry a mutation in their genotype known to cause a disease, they can potentially donate their cells to create disease-specific iPSC lines. As an example, the first iPSC-derived disease cell lines were for genetic heart conditions like Long QT, LEONARD, FHCM, dilated cardiomyopathy (DCM) [29]. Apart from the recapitulation of the patient-specific pathophysiology, these disease models also can be used to recapitulate drug response [32]. This makes it possible to assess drug quality, effectiveness, and possible toxicity without administering the drug to an actual patient. This drug assessment method has been shown effective in e.g. beta agonists and beta blockers because the patient-derived cell lines respond similarly to the drug as the actual patient itself. This type of research is crucial because of the possibly fatal effect they can have in patients with heart failure (HF) [29].

To effectively monitor the efficiency of several drugs, the disease model must have a correct physiological drug response. That means that the used cell line must have a similar response to certain drugs as in patients [29].

These models of cardiovascular diseases (CVDs) can be used in 2D and 3D cultures. The following section will discuss 3D cultures. Previous studies have already shown the possibility of disease modeling with the use of hiPSCs in 2D cultures, where several parameters like cell morphology, contractility, and calcium handling can be analyzed, also in context with FHCM [33].

Also, other kinds of diseases have been reported to be successfully modeled in a 2D format using hiPSCs. Like in non-CVD-related diseases like metabolic deficiencies in the liver using patient-specific hepatocytes. [34]. Other examples are the modeling of Parkinson's Disease, where dopaminergic neurons from patients are cultured and successfully were exhibiting increased oxidative stress, and impaired mitochondrial function [34]. Furthermore, with the CRISPR-CAS9 genome editing technology, cell lines can be altered with the insertion or deletion of specific mutations to induce mutation-induced diseases to the cell line [34].

1.7 Differentiation of hIPSCs to CMs

As stated above hiPSCs can be differentiated into almost any cell type. For successful differentiation from hIPSCs to CMs, there are certain crucial factors. The initiation of differentiation is generally done by activation of the WnT signaling pathway. This can be done by the administration of GSK3 inhibitors[35]. hiPSC CM differentiation techniques used in this research are the same as done by [36, 37]. Initiation of differentiation is done in BPEL (BSA, Plyvinylalcohol Essential Lipids) supplemented with low insulin with additional growth factors like BMP4, CHIR99-21 (the activator of the WnT signaling pathway) and Activin A. Which is also described by [11]. After initiation, hiPSCs usually take 13 days to be fully differentiated to CMs.

1.8 Purification of hIPSC derived CMs

Previously documented hiPSC-CM differentiation protocols reported an expected yield of 30-45% of CM at day 16 of differentiation [38, 39]. CM differentiation nowadays is 70-80% effective, but can still vary per cell line [40]. With a purification protocol, CM generation can be optimized to get a much higher yield (90 %). This purification is based on the differences in metabolism from other mammalian cells and CM. Non-CMs use glucose as their main energy supply. However, CMs can get their energy from different sources, like lactate.

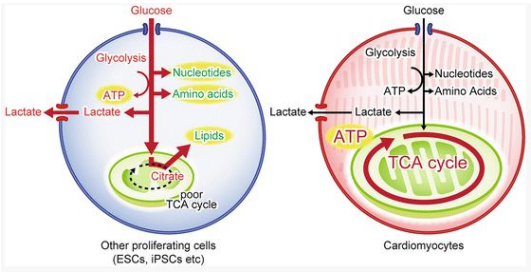

Figure 4: Differences in cellular metabolism between CMs and other cells, CMs can rely on the TCA cylce, while other cells cannot [41]

Figures 4 and 5 show the differences in metabolic properties between CMs and non-CMs. The main energy source of most mammalian cells is glucose. CMs can get their energy from other sources like fatty acids and lactate [39]. Compared to other mammalian cells, CMs express more genes promoting the use of the tricarboxylic acid (TCA) cycle. By culturing the CMs with lactate as the main energy source instead of glucose, the cells are forced to get their ATP from the TCA cycle, causing only the CMs to survive.

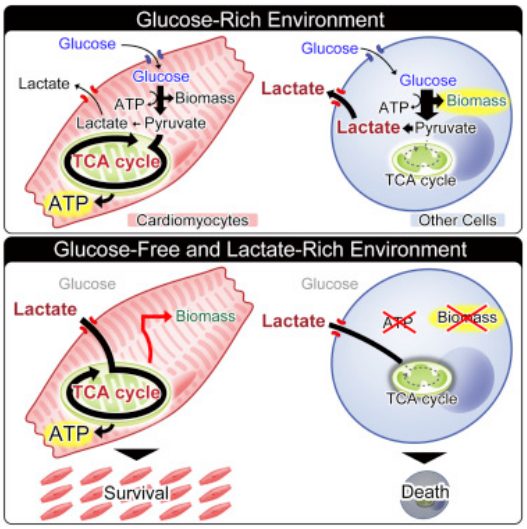

Figure 5: Metabolism of CMs and other cells in a glucose rich and glucose free and lactate rich environment, it is shown that only CMs proliferate in a lactate rich environment [42]

1.9 CRISPR-CAS9 genome editing

CRISPR-CAS9 genome editing technique can be used in combination with hiPSCs to induce mutations in the hiPSCs to give us deep insight into the molecular bases of many diseases and for pharmacological research purposes, and with that facilitate and improve disease models. Applications of hiPSCs as stated above can be associated with gene editing, to gain more understanding in the pathophysiology and carry out drug screening and disease modeling [43]. CRISPR-CAS9 is a gene-editing tool to write, remove and correct genetic information in a DNA sequence.

CRISPR is an abbreviation for Clustered Regularly Interspaced Short Palindromic Repeat DNA sequences. The technology relies on an endonuclease protein whose DNA can be programmed

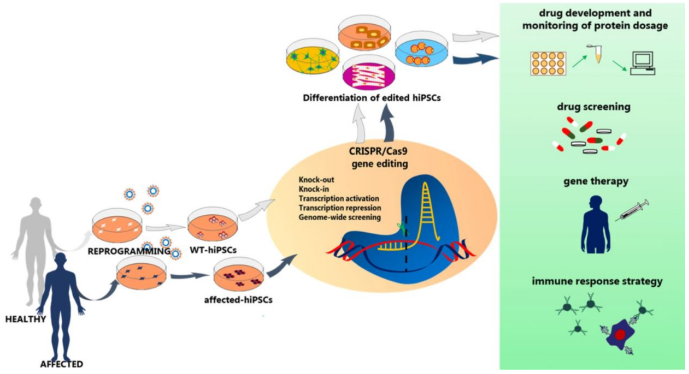

Figure 6: CRISPR-CAS9 genome editing technique in combination with hIPSCs can lead to new drug discoveries and drug screening [43]

by RNA to modulate its specificity and cutting activity [44]. The system is adapted from the genome editing naturally occurring characteristics of genome editing in bacteria, which capture little pieces of DNA strands from viruses and re-use those strands to create new DNA segments which are known as CRISPR-arrays [45]. This phenomenon is then used in the lab to create cell cultures with induced genetic mutations. A piece of RNA is created with the desired specificity and cutting activity, that attaches to a target sequence of the DNA in the genome of the target cell. This piece of RNA binds to the enzyme Cas9, when the RNA recognizes the DNA sequence, the Cas9 enzyme cuts the DNA at the specified location. Then, a new strand of DNA is added in between those pieces of DNA (which can be a strand of a genetic mutation for a specified disease). After this, the genome of the cell is permanently altered, and now expressing a different phenotype [45]. Figure 7 shows a schematic overview of the CRISPR-Cas9 genome editing technique.

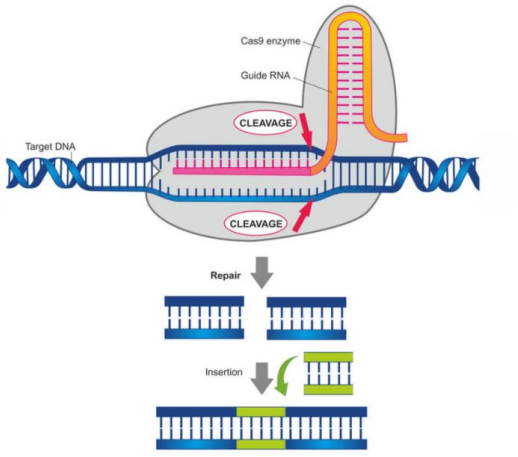

Figure 7: Schematic and simplified overview of CRISPR-CAS9 technique [46]

1.10 hiPSC based 3D disease models

However 2D hiPSC based models have been shown to successfully mimic some of the key characteristics of a series of diseases, they still have some major limitations. One of these is that 2D cultures are generally immature and resemble fetal cells rather than their adult cell counterparts. To account for these limitations, engineered heart tissues (EHTs) will be used in this research.

1.11 Human engineered heart tissues

EHTs consist of CMs and potentially other cell types like fibroblasts (FBs) and endothelial cells (ECs). Cells are seeded in a 3D organization most commonly cultured in a 24 well plate. They are widely used in previous research because they can overcome limitations with more commonly and wider used (static) monolayer cultures of CMs. The main limitation of these monolayer cultures is their inability to easily co-culture them with other types of cells and their poor representation to the *in vivo* environment.

EHTs have been used extensively for the last decades to create mature and functional heart muscle. In the first reports of EHTs, they were derived from neonatal chicken CMs with the use a of collagen matrix to form gelated EHTs [47]. Zimmermann et al. [48] reported on the use of neonatal rat CMs with the use of collagen as extracullular matrix (ECM) factors to generate ring-shaped EHTs. Later, they emerged to a fibrin/thrombin-based ECM also using neonatal rat CMs [49].

Research conducted by Schaaf et al. [50] used embryoid bodies (EBs) from hESCs for the generation of EHTs in a 24 well construct. This study used a PDMS rack that is a construct for supporting four tissues (one tissue per well). Research conducted by Breckwoldt et al. [51] follows up on this study. Where the EHTs are made using hiPSC derived EBs. This approach also uses a large PDMS rack mold where only one EHT can form within a well, this is shown in figure 8. The same 24-well format is also used by Hirt et al. [52]. In these studies, only one EHT can be produced per well, and roughly 600k CMs are needed to form one EHT. This makes this method time consuming, low throughput and quite expensive. High throughput is very desired for the type of research that is conducted with EHTs.

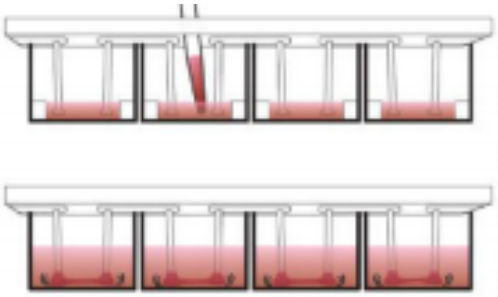

Figure 8: Engineered Heart tissue as described by [51], generated with one tissue per well and 4 tissues per PDMS construct

Furthermore, more EHTs derived from hiPSCs exist [53, 54], stating that the use of hiPSCs usually is limited by their immature state. Lomoine et al. [53] compared EHTs to traditional 2D culture in terms of upstroke velocity and sodium current density and reported greater resemblance to human heart tissues in the EHT configuration.

Not only non-specific CM-based EHTs are used for disease modeling, research by Lemme et al. goes a step further by engineering atrium-specific EHTs [55]. This study used hiPSCs to form EHTs using differentiated right atrial cells. Using these models, atrium-related heart conditions like atrial fibrillation can be studied in an EHT format.

Goldfracht et al. [56] make use of ring-shaped EHTs as described in [48] with hiPSC-CMs, using ECM from decellularized pig hearts enhanced with chitosan. They also use the ring-shaped EHTs in further research [57], differentiating the stem cells into atrial- and ventricular-like cells. Then the CMs were embedded into a collagen hydrogel where they formed ring-shaped EHTs in the presence of casting molds, which are also chamber-specific [57]. This gives rise to a new generation of EHTs, which make it possible to study heart disease on a chamber-specific level. Figure 9 shows the generation of the ring-shaped EHTs.

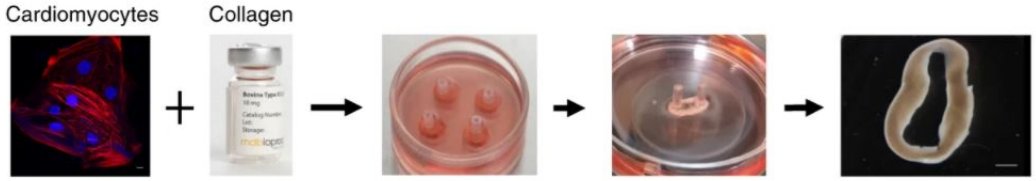

Figure 9: Generation of ring shaped EHTs as described and depicted in [57]

1.12 Engineered heart tissues vs. 2D cultures

Thus, many hiPSC 2D/3D models of different diseases exist and are very suitable for modeling different heart-related diseases [58, 59, 60]. 2D models lack a good representation of the 3D ECM, and important cellular networks [51]. Many of those 2D models fail to see contractile deficits in their 2D environment, but it can be visible in a 3D construct, like in the research of Hinson et al. [61], where this phenomenon happened with a model of dilated cardiomyopathy (DCM). Furthermore, it has been shown that hiPSC derived EHTs show more mature properties than their 2D counterparts. Yang et al. [62] also reported differences between 3D hiPSC derived EHTs and conventional 2D culture and observed more cell/cell ECM interactions and more interaction with the microenvironment, better paracrine signaling and superior energy metabolism in the hiPSC derived EHTs, suggesting a superior representation of the *in vivo* environment. Also, a higher expression of several ECM proteins and genes was observed [63]. Furthermore, the main reason for using EHTs vs. 2D culture in this research is that 2D cultures have a primitively developed sarcomeric organization of myofilament, which is a good indication of CM maturity. Therefore the contraction force of these cells cannot be evaluated in a precise and reliable manner. This has to do with the absence of an auxotonic load which the cells have to work against. This auxotonic load is provided to the EHTs in the form of the flexible PDMS pillar, which can be seen in figure 10 [51, 49]. Generally, hiPSC-CMs in EHT format show a higher level of maturity.

1.13 EHT format used in this research

In this research, we make use of a unique polydimethylsiloxane (PDMS) based pillar system that can hold up to three EHTs per well in a 12 well plate. The PDMS material is used for its flexibility and tunable characteristics. The way that the pillars and EHTs are generated can be read in the materials and methods section. The PDMS pillars consist of a base, with six pillars and PDMS plates at the bottom of the pillar. When cells are seeded around these pillars, they can start to contract and pull the flexible PDMS pillars towards each other, causing a displacement, the principle is shown in 10 . The tissue will stay in place due to the plates at the bottom of the pillar. The pillars are exerting an auxotonic force on the CMs which will make contraction analysis possible. This displacement can be recorded with additional software. Knowing the Youngs modulus of the PDMS, the force of contraction can be extracted from this.

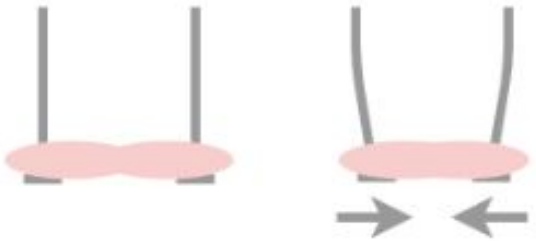

Figure 10: Schematic representation of the pillars with heart tissue seeded around. Left: relaxed Right: contracted

1.14 Going smaller, µEHTs

For the better in *vitro* mimicking of cardiac disease models, it is desired to make a disease model that is as biomimetic as possible. As the current standardized EHT format is now a static culture and not able to incorporate fluid flow, it is interesting to look at alternative ways to form EHTs. Previous research by Vollert et al. [64] stated that constant perfusion of EHTs improved cell density and tissue homogeneity. Kolanowski et al. [65] also showed increased alignment and contractility of hiPSC-CMs in a microfluidic and constantly perfused environment. It also leads to an increase in mitochondrial network density and increased maturity of the cells. Wei et al. [66], reported on the use of perfusion-based hiPSC-CM culture, which improved the viability and calcium response of the tissues and can improve the hiPSC-CM metabolic maturity [67]. Perfusion cultures will also expose the EHTs to shear stress, which can improve the sarcomeric alignment. It is also known that dynamic hiPSC-CM cultures improve the maturity and functional output of the CMs [68, 69]. Another important limitation of the standardized EHTs is that they are prone to handling errors and require many cells per tissue (about 800k CMs per 3 tissues), which makes them relatively expensive to produce. To account for those limitations, the µEHT format is studied here. Experiments for modeling FHCM were carried out with the standard EHT format, as those are standardized and working. The µEHT format is still experimental. The µEHTs are seeded onto a microfluidic chip consisting of four tissue chambers connected to a top channel and a bottom channel. Inside each chamber, two flexible PDMS pillars are present where the tissue can form around. Because the pillars are smaller than those in the regular EHT format, a smaller amount of cells is needed to form a tissue. This is explained further in section 3.12.

1.15 Cardiac micro-environment

As mentioned above, one of the limitations of the static monolayer cultures is that they lack the ability to be co-cultured with different cell types to form complex multi-cellular constructs that exist within the *in vivo* cardiac microenvironment.

Like all other organs, the heart is a multi-cellular organ consisting of a complex microenvironment, with each cell influencing the heart's function in sickness and in health [70]. The main cell types that we focus on in this research are CMs, FBs, and ECs. The primary function of the CMs is the generation of contraction and the electrical conduction, causing the rhythmic beating in the heart. As stated above, other processes like vascularization, maintenance of the extracellular matrix, inflammation, and autonomic regulation have to be taken care of as well to be able to create a biomimetic model [70]. So the interactions between the CMs and the cells from their microenvironment are critical for in *vivo* functionality of the heart and thus for the in *vitro* modeling of the heart.

Cardiac FBs have multiple functions within the heart. They play roles in the remodeling and development of the heart, and have a role in defining structure and function, because they play a crucial role in the production of extracellular matrix (ECM). Also, their role in mechanical and electrical signaling is believed to contribute to ventricular contraction [71]. This is believed to be done partly by the expression of so-called connexins. In cardiac repair, they play a role in the inflammatory response to injury to the myocardium [71].

Cardiac ECs have a role in maintaining the structure of the surface of blood vessels and regulating the angiogenesis [72]. Angiogenesis is mainly controlled by the secretion of Vascular Endothelial Growth Factor (VEGF) [73], which is secreted by the CMs. In their turn, the ECs promote myocardial development by sending signals. For example, ECs account for the deletion of platelet-derived growth factor (PDGF), which can cause abnormalities in cardiac development. Also, crosstalk between CMs and ECs partly relies on cardiac angiocrines. The primary function of ECs is angiogenesis. In this process they secrete many factors and sets of proteins [72]. These so-called angiocrines act on their neighboring cells and thus on CMs. An example of one of these factors is NO, which can act on the vasculature of CMs, and with that can act on the contractility of CMs. Also, crosstalk has been identified with the substance Endothelin-1 [72]. This is a substance that ECs, CMs, and cFB secrete to regulate contractility and cardiac remodeling. Where the CMs in the myocardium are connected physically, they communicate between different paths, like gap junctions and desmosomes.

Thus, CMs and FBs are the main constituents of the human myocardium. CMs are estimated to account for +- 30% of the total cell number in the heart. Saini et al. [74] showed that 3D cardiac models using rat CMs co-cultured with FBs will improve those tissues with respect to protein expression, organization and synchronicity of beating. Rupert et al. [35] make use of hiPSC derived CMs and FBs for improving 3D engineered tissues, and indicated 5% FBs benefited the engineered tissues the most. They reported improvement of the formation of the tissues, contractile function, and material properties. Giving the overall impression FBs will improve the maturation, formation, and mechanical properties of EHTs. Giacomelli et al. [75] also showed enhanced maturation in 3D cardiac tissues using FBs and ECs, with improved contractility and sarcomeric structures. Making FBs and ECs co-culture an exciting option for improving the EHTs in this research.

1.16 Hypertrophic stimuli for modeling cardiac hypertrophy

Several compounds can be used for the modeling of cardiac hypertrophy rather than the use of cell lines. Commonly used compounds are Isoprotenerol and phenylephrine (PE) [36]. In this research, PE was used for exploring the possibilities of disease modeling. PE acts as an alpha agonist. It works mainly as a vasoconstrictor in the pulmonary and cardiac region [76], thereby increasing systemic arterial and venous pressure leading to vascular resistance. It is also known to decrease heart rate and either increase or decrease cardiac output [36, 77]. In the clinic, it is often used to treat hypotension [78]. Foldes et al. [79] reported on PE-induced cardiac hypertrophy increasing the cell size 1.5 fold, giving the impression that PE can be used for the modeling and the modulation of cardiac hypertrophy. Furthermore, PE is used in various studies to research simulated cardiac hypertrophy. Peng et al. [80] used PE in mouse models, showing a decreased rate of survival and an HF rate up to 90% over the course of 12 months. Furthermore, they were able to study the effects of anacardic acid to treat PE-induced hypertrophy. PE-induced hypertrophy is also researched in hIPSCs cultured CMs in 2D cultures. Rupert et al. [81] used a concentration of 2µL of PE to induce hypertrophy in hiPSC derived CMs and reported an increase in cellular area. All of this taken together, PE is a good candidate for studying its hypertrophic effects in EHTs.

2 Aim of the research

As well-defined biomimetic 3D disease models for FHCM are still lacking [11], this research will focus on developing a model using hiPSC derived CMs. The hiPSCs have been genetically modified with CRISPR-CAS9 to induce the mutation in the MYBPC3 gene (c.2373dupG) [5, 11]. We will model this using EHTs, which aims to give a good comparison of the difference in contractile parameters between a control cell line and mutated cell line. The model will be made with un-purified CMs and lactate purified CMs, to see if purification will give a more precise representation of the disease phenotype due to a higher % content of CMs [42]. Given that PE is a generally used compound to induce hypertrophy in hiPSC models [81], we will test the effect of PE stimulation on EHTs to see the effect on the contractile parameters of the EHTs and see if it has a similar effect on the contraction as the MYBPC3 mutation. Furthermore, the possibility of EHT culture in microfluidic conditions will be researched, give the option of dynamic culture and usage of a lower amount of cells, and increase the future throughput of EHT-based disease models. To better mimic the *in vivo* environment, we look at the co-culture of CMs and ECs, to see if there are differences in contraction and formation. All of this taken together, this research will have the following aims:

- Can we create a disease model of FHCM using EHTs and hiPSC derived CM cell lines with a mutation in the MYBPC3 gene (c.2373dupG)?
- Can we observe contraction differences between a healthy control and a mutated CM cell line?
- Can we use lactate purified hiPSC-CMs to obtain a similar disease model for FHCM with the mutated MYBPC3 cell line vs. the healthy cell line and can we see contraction differences between them?
- Is it possible to use hypertrophic stimuli, like PE, to model hypertrophic effects and possibly HF on EHTs?
- What is the influence of using a different type of EHT, using a different platform and fewer cells, combined with the use of ECs on the contraction pattern and formation of the EHTs

For the MYBPC3 cell line vs the control (FLB) cell line, a significant decrease in contraction/relaxation force is expected as well as decreased contraction/relaxation times and velocities [11, 82, 18]. As this model will mimic the diseased cardiac tissue, and previous research has shown a significant decrease in contractile force in MYBPC3 mutated iPSCs as shown in [83, 11]. The same trend is expected in the tissues using lactate purified CMs. The expectation is that the models with lactate purified cells will perform better in terms of difference in contraction pattern, because of the expected higher CM content compared to the un-purified CMs [41, 39]
For the PE experiments, we expect a hypertrophic response in the EHTs and a decreased force of contraction as well as a decrease in contraction and relaxation force, mimicking a FHCM model.
In the case of the µEHTs, a more robust structure and better formation are expected when ECs are present as well as improved tissue survival [64].

3 Materials and Methods

In this section, we will go over the materials and methods for the experiments conducted. We will first discuss the different cell lines that are used in the experiments. We will also go over the

generation of the EHTs, where the generation of the PDMS chips (pillars) for the EHTs will be discussed followed by three different methods of HCM/HF disease modeling (using un-purified CMs, purified CMs, and PE stimulation). These models will be evaluated by their contractile properties. Then, we will look at the chip generation of the µEHTs followed by the experiments conducted with the µEHTs, which involve co-culture with ECs and will be evaluated by their formation and contractile properties.

3.1 Used cell lines

In the different experiments conducted, we make use of different cell lines. Two of the cell lines arise from hIPSCs and one cell line from derived from ESCs is used.

- The FLB CM cell line, which is a healthy cell line serving as control, derived from hIPSCs reprogrammed from primary skin FBs as done in [84]
- The MYBPC3 CM cell line, which is a mutated cell line from the same origin and differentiation as the FLB cell line, with a CRIPR-CAS induced mutation in the MYBPC3 gene, used to recapitulate the FHCM phenotype
- COUP-TF II is a reporter cell line (chick ovalbumin upstream promoter transcription factor II) derived from hESC. It is a dual atrial reporter cell line which is expressing GFP from the NKX 2.5 locus [85].
- The cFB cell line, all of the cFB used in the experiments are derived from hIPSCs and were available in our lab
- The cEC cell line, all of the cECs used in the experiments with the µEHTs are derived from hIPSCs and were available in our lab

All cells used in this research are cells frozen in LN after differentiation. All of the ECs come from the same batch. Moreover, the FBs come from different batches but are all derived in the same fashion.

3.2 Composition of culture medium

Used medium for EHT cultures generally consists of basic CM medium (contents can be found in supplement A) supplemented with T3 hormone (100nM) Dexamethasone (1µM) and IGF (100ng/ml). For working with purified cells, the medium also contains lactate (4.5mM) and low glucose (4.5mM). For working with non-purified cells, it contains 10% horse serum (HS) and low glucose (4.5mM). The medium cannot be used to form the tissues approximately one week after adding the TDI supplements because of their stability. For the experiments using ECs medium is supplemented with SB50 (10µM) and VEGF (50ng/mL).

3.3 CM Purification

The lactate purification is done by switching differentiated hiPSC-CMs from basic CM glucose-rich medium to no glucose medium supplemented with 5mM of sodium D-L lactate solution (60%, Sigma Aldrich, cat. no. L4263) on d13 of culture of the beating CMs until d17 and refreshed daily. On day 17, purified CMs were kept in lactate purification medium supplemented with 4.5mM of glucose until d20. On d20, cells are dissociated with triple 10X (ThermoFisher, A1217702) and frozen in LN. Lactate purification done with the FLB cell line is the same as for the COUP TF-II cell line.

3.4 Thawing of the cells

The cells used in the experiments are not fresh from culture, but instead from cells frozen in LN. The age of the cells varies per batch. Cells were thawed in a warm water bath at +- 32*C while stirring to ensure the vial was thawed uniformly. Cells were then diluted further with Dulbecco's modified eagle medium (DMEM) and transferred to the preferred medium after spinning down and removing thawing medium and DMEM. For the CMs, addition of DMEM has to be done drop by drop, as immediate adding of the entirety of medium will kill a portion of the cells due to calcium shock. While working with FBs and ECs, the DMEM is added slightly faster. When thawing is complete, cells are spun down and transferred to the medium in which they will eventually be cultured in the EHT format of choice.

3.5 FACS analysis

The CM content in the lactate purified cells is evaluated by fluorescence-activated single cell sorting (FACS). The sample for FACS is taken right before the moment that the EHTs are seeded and have to contain a minimum of 100k cells for an adequate analysis. FACS sorts cells based on their interaction with laser light in a flow cytometer. The main characteristics of the sorted cells are their fluorescence and light scattering. Because of this, the CMs are separated from rest cells, and the percentage of CMs can be determined, showing the effectiveness of the lactate treatment. The expected and desired CM yield will be around 90% for the lactate purified CMs [42]. To check the purity of the FLB cell lines, cells were stained with cardiac troponin T. For the checking of the purity of the COUP-TFII reporter line, we look at the percentage of cells expressing green fluorescent protein (GFP).

3.6 EHT chip generation (pillars)

The generation of EHTs chips is a three-step process. The used material is PDMS which consists of a 10:1 elastomer (Sylgard 184):curing agent (Sylgard 184) ratio. The three-step process starts with the generation of the pillars themselves, followed by painting of the pillars, and finally the generation of plates underneath the pillars to support the EHTs and prevent them from sliding off the pillars, which will be discussed further in this section. All discussed EHT molds are made by José Arbelaez.

The PDMS bases of the pillars are generated by using a mold that can make 30 PDMS bases at once. The mold is micro-milled from Teflon. Due to the hydrophilicity of the Teflon, the PDMS can detach after curing. Figure 11 shows the mold and PMMA box. The mold contains six tiny holes per base to form the pillars, and four elevated tips on top to form holes that make attachment to the well plate possible. PDMS is cast in a custom made PMMA box and filled up until the top tips are just about covered. After casting, the box needs to be degassed thoroughly to remove the bubbles from the pillar holes. When bubbles stay in the pillar holes, the pillars have a chance of forming incompletely. The whole box is cured overnight in the oven at 65*C. After curing, the PDMS is cut out to form 30 PDMS pillar bases.

The second step is painting the PDMS pillars, which is done by dipping them in black PDMS (ratio 10:1 Elastomer:Curing agent). The black PDMS is made by adding 2.1g of carbon to a 50mL tube of PDMS. After painting, the pillars are put in a 12 well plate with holders and cured for 90 minutes in the oven at 65*C. After curing, the painted pillars need to be checked for height and uniformity of the painting. Height differences can result in difficulties with plate forming and

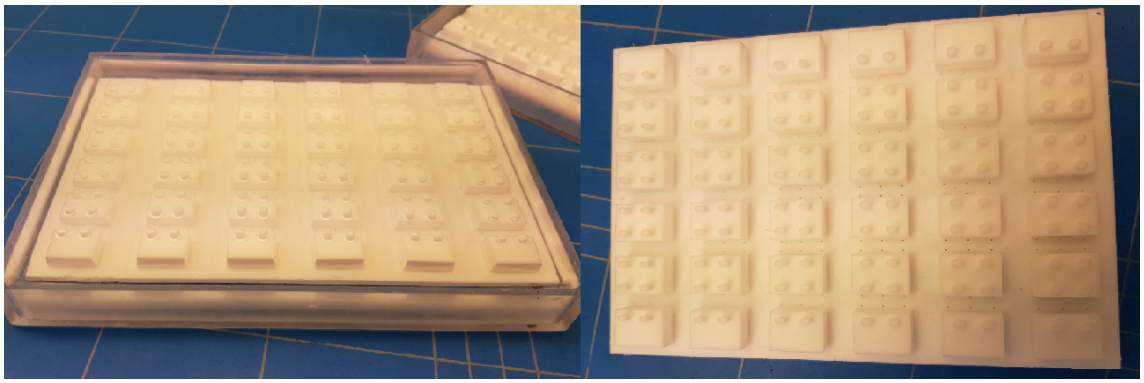

Figure 11: Right: The Teflon mold from which 30 PDMS pillar bases can be formed. Left: The Teflon mold in the PMMA box before casting PDMS

inconsistently painted pillars, resulting in difficulties analyzing the tissues. The contraction analysis software needs clear black tips to detect the contraction pattern of the EHTs, which will be discussed further in section 3.16.

The third step is the generation of plates, which is done by putting the painted (or unpainted) pillar in a PMMA mold. This mold is also made by micro-milling (Figure 12). The mold consists of two parts. The first part is for keeping the pillars in place and can hold up to ten pillars at a time. The second part is a rectangle plate with two grooves for mounting the top part. For every pillar, there is a circular hole in which the pillar fits. The holes need to be filled up with PDMS manually, using for example a pipette tip. After filling up the holes, excess PDMS is removed, and the top part can be shoved in and adjusted to the correct configuration to ensure a maximum effective outcome. This is still a tricky part, which only yields around 75% usable pillars. A picture of the different parts of the mold is shown in figure 12.

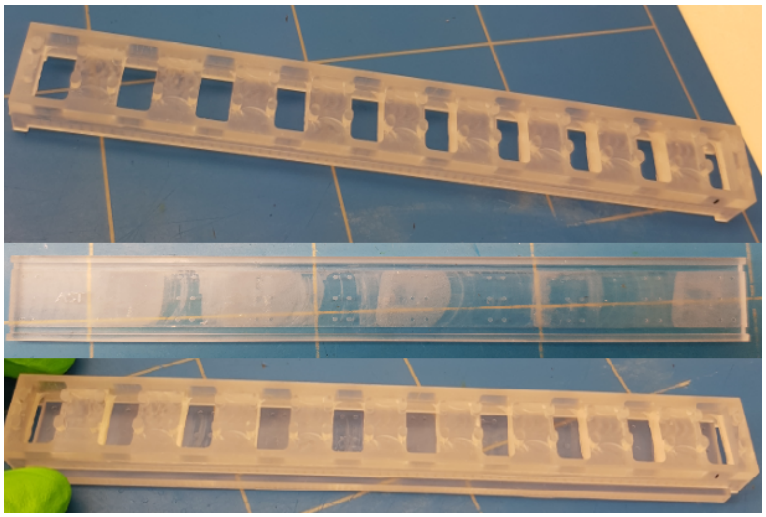

Figure 12: The parts of the mold to make the pillar plates. Top: part that holds the PDMS base. Middle: Part in which PDMS is cast in holes to form the plates. Bottom: The two parts put together.

Figure 13 shows the finalized pillars. The six separate pillars can be seen. The EHTs will form around two adjacent pillars (from left to right). After formation, the heart tissue will start beating which can be monitored using software detecting the black dots, which will be discussed in

section 3.16. The plates are well centered and will prevent the tissue from sliding off the pillars.

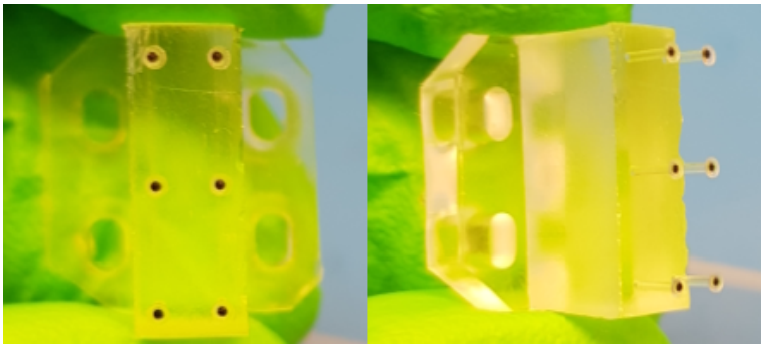

Figure 13: The final turnout of the pillars after the design process described above

3.6.1 Pillar attachment to the well plate

For the attachment of the pillars to the well plate, a specific holder is used. This holder is made from COC. The custom-made holder fits in the well perfectly and holds the pillar in place with four tips that fit in the four holes of the PDMS pillar. Figure 14 shows the COC holder. The COC holder is designed so that it perfectly fits each position on the 12 well plates. So all 12 wells of the plate can be used to hold three EHTs per well. So a total of 36 EHTs can be cultured per 12 well plate.

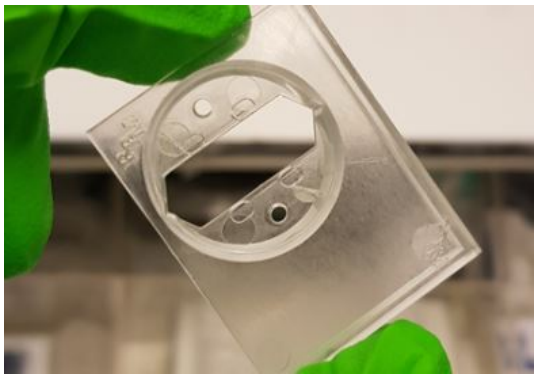

Figure 14: The COC holder which can hold the PDMS pillars, when the pillar is put in the holder, it can be put into the 12 well plate

3.7 Sterilization of the pillars and holders

Before the pillars (and pillar holders) are used for experiments with living cells, they need to be sterilized to prevent contamination of the cultures. This sterilization is done by the CUTE plasma cleaner. The pillars and holders are exposed to a plasma cleaning treatment cycle of approx. 6 minutes, whereas 40 seconds is actual exposure to the plasma.

3.8 Well plate preparation

Agarose molds must be formed inside the well plate to ensure the EHTs can be appropriately formed. The used plates are 12 well cell culture plates from Sigma Aldrich. The wells are filled by 1.2mL of medium containing 10% of agarose. The medium consists of basic CM + supplements (depending on the experiment). After putting the agarose medium in the wells, holders and Teflon spacers are put in. The Teflon spacers are sterilized by autoclaving. The spacers have three cutouts to make sure every well can hold three EHTs. The molds are being held in the freezer or the fridge for approx. one hour to make the agarose solid. After that, the spacers are removed, and molds can be stored (when needed) in a freezer at -20*C. To keep the molds as intact as possible, it is desired that the molds are frozen while they rest on a straight surface. One hour before using, the molds are moved to a fridge at -4*C. Before the addition of the cell suspension, excess agarose inside of the holes is aspirated to prevent pillars from bending inside of the well. The bending of the pillars has a negative effect on the formation of the EHTs. Figure 15 shows a picture of the agarose molds.

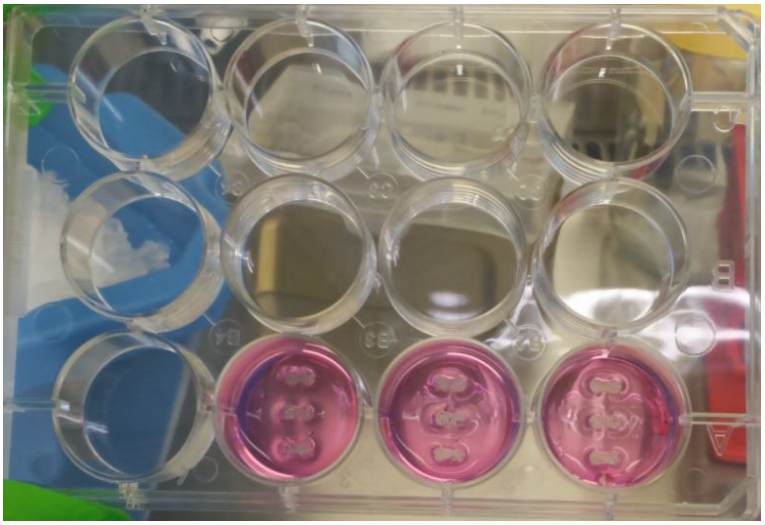

Figure 15: Picture of three agarose molds in a 12 well plate, made by using 1.2 mL of agarose medium in combination with the custum made spacers

3.9 EHT generation

As stated above, the main cellular constituents of the EHTs are CMs, FBs, and potentially ECs. The generation of the EHTs is done in the agarose molds as described in section 3.8. In one well, three EHTs can be generated. The three holes in the mold can each hold 15µL of liquid consisting of cell suspension (70%) and:

- **Fibrinogen (10%, 20mg/mL)** -> Fibrinogen is the most important component of the mastermix, as this is the solution that provides the scaffold of the EHTs.
- **2X medium (10%)** -> The 2X medium is basic CM medium with two times the concentration of its normal components. The 2X medium is potentially supplemented depending on the medium that is used to culture the cells and EHTs. The 2X medium is used to compensate for lack of salts in the fibrinogen (which is diluted in water).

- **Matrigel (10%, 100µL/mL)** -> Matrigel is used as a basement membrane to promote the formation of the EHTs. Matrigel is a mixture that resembles extracellular environment.
- **Aprotinin(1:100 % 250µg/mL)** -> Aprotinin is present to prevent the degradation of the fibrinogen based matrix, and will keep the EHTs intact for a longer period of time.

Thrombin (20U/mL) (1:242,42) to amount of fibrinogen is then added, which will cause the fibrinogen to coagulate and gelate so the EHT can form. Timing is an important factor here. After the thrombin is added to the cell-mix suspension, the mixture will gelate in about 4-5 minutes, making it unable to be pipetted in the agarose molds. This makes it important to use the right concentration and amount of thrombin for the amount of tissues that are being made in one go. When the 15µL of solution is pipetted into the agarose molds, the pillars in the holders are pressed into the well plate. EHT formation takes around 10 minutes, whereafter 1mL of medium is added to each well, and the plate is incubated at 37*C. A timeline of hiPSCs until the moment of EHT measurement can be found in the supplementary material (figure S1)

Figure 16 shows the generation of the agarose mold with the Teflon spacer and how the PDMS pillars fit inside of this mold in the 12 well plate. (f) show the tissues around the pillars inside of the well.

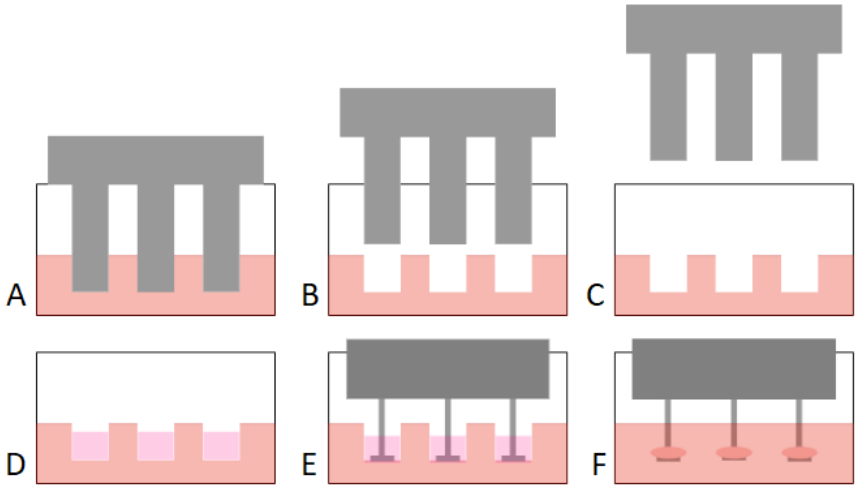

Figure 16: Generation of agarose molds and EHTs. A: Agarose mold with Teflon spacer inside of the well B: Telfon spacer begin removed from the agarose after freezing C: Teflon spacer fully removed leaving only the agarose inside of the well D: Cell suspension as described above inside of the agarose E: with PDMS pillars inside F: After incubation, melted agarose and formed EHTs around the PDMS pillars inside of the well

Figure 17 shows the pillars with the EHTs from a front view and shows the importance of the pillars and plates.

3.10 EHT maintenance

After the regular EHTs are generated, they will be maintained by medium refreshment by pipetting out 1mL of old medium and pipetting in 1mL of fresh medium. This has to be done carefully, to prevent damage to the EHTs and the PDMS pillars. The EHTs are refreshed on the day after they have been made. Then refreshed every two days. One day before measurement, the EHTs will be transferred to a new 12 well plate with 2mL of fresh medium per well. The clean

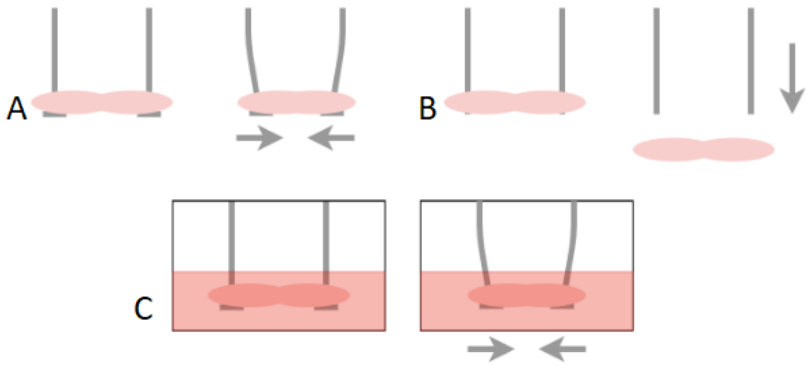

Figure 17: Front view of the pillars with compacted tissue around them A: Contracting EHT with pillars flexing towards each other creating a displacement due to auxotonic force exerted by the PDMS pillars B: Importance of the plates, when there are no plates present, the tissue will slide off C: Contracting EHT inside of a well

well plate has a positive effect on the quality of the microscopic measurements and imaging. As the EHTs are matured for approx. 10 days in the same well plate, it is bound to get foggy and dirty (especially from the outside). And because of this, the contraction analysis software may have a hard time detecting the contracting tissue.

3.11 FHCM HF model experiments using EHTs

For the FHCM HF model using un-purified cells, EHTs are cultured in medium described in section 3.2. The control line is FLB cell-line CMs un-purified (800k cells per well) and cFBs (5% = 40k cFBs per well). And for the FHCM HF model, the MYBPC3 cell line is used (800k CMs per well) and cFBs (40k per well). As discussed before, one well can can hold three EHTs.

For the FHCM HF model using lactate purified CMs, EHTs are cultured in lactate purification medium as described in section 3.2. We also make use of the FLB cell line as a control (800k cells per well) and cFBs (40k cFBs per well), and the MYBPC3 cell line (800k cells per well) and cFBs (40k cFBs per well). Three different batches of cells were used in these models. A batch from May 9th, June 7th and June 22nd. These batches contain the cell lines of FLB and MYBPC. They will be compared in terms of contraction force. Before EHT formation, at least 100k cells per cell-line/batch will be taken for FACS analysis, to assess the percentage of CMs in each of the samples. This way we can see how the EHTs perform with respect to each other in terms of contraction force between different cell lines and percentage of CMs.

For the disease model using hypertrophic stimulant PE, EHTs are cultured in lactate purification medium described in section 3.2. The used cells are lactate purified FLB (800k per well) and 5 % FBs (40k per well). Per experiment, a total of four wells each containing three EHTs are made. After EHT maturation at day 10, different concentrations of PE are added up to d17. The used concentrations of PE are 0µM (control), 20 µM, 100 µM and 200µM. Imaging and contraction measurements are done at D17 after adding PE to the wells on a daily basis (with the exception of the weekends). Per condition, nine EHTs are expected.

3.12 µEHT chip generation

The chip generation of the µEHTs is a multi-step process. The chips consist of 2 separate parts. The first part is the PDMS part of the chip. Which is generated using a custom-made mold. The material of the mold is Teflon. Figure 18 shows the mold in which the PDMS µEHT chips are made. The mold can produce ten chips at once. To make the chips, tape is put on the sides to form a tub, and PDMS is cast inside. The PDMS is cured for a minimum of 12 hours at 65*C. After curing, chips are cut out and inlets/outlets of 1mm in diameter are punched using a biopsy puncher.

Figure 18: The mold used for generating the PDMS part of the µEHT chips

The second part of the chip consists of a glass microscope slide which needs to be bonded to the PDMS part of the chip. To ensure maximal bonding strength, a thin layer of PDMS (1.5mL) is spin-coated onto the glass slide. After spin-coating, the glass slide is cured in the oven at 65*C for at least 1 hour.

The third step of the chip fabrication process is bonding. For plasma bonding, the chip and the slide are plasma treated in the CUTE plasma cleaner for 6 minutes, 40 seconds of which is the actual plasma treatment. After the treatment process, the PDMS part and glass slide are bonded together creating a chip as shown in figure 19.

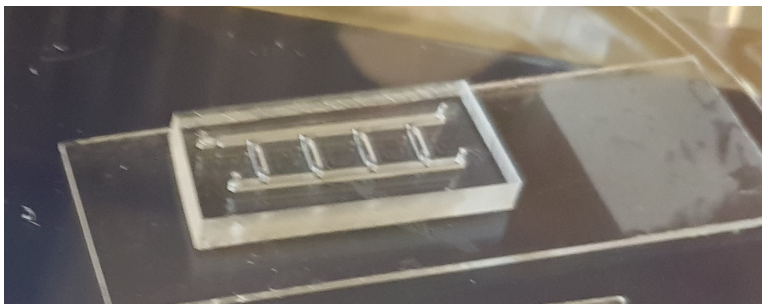

Figure 19: The finalized µEHT chip with the PDMS part on top and glass slide at the bottom

3.13 µEHT formation

Before working with cell solutions, the chips need to be treated with pluronic f127 (1% in H2O) to prevent the adhesion of cells to the walls of the chip. Before the seeding of the cells, 60µL of pluronic f127 is pipetted into the top channel until all chambers and the top channel are filled. The pluronic needs to be incubated for at least 30 minutes but is generally removed after +- 2 hours. Before working with cells, pluronic is aspirated from the chip using a vacuum pump system. It is important that all the pluronic is removed.

A detailed protocol for the formation of µEHTs is provided in the supplementary material (supplement B). To be able to fill up one chip with cell/mix solution, 60µL is needed to fill up all four chambers. The solution contains 70% cell solution, 10% fibrinogen (20mg/mL), 10% matrigel (100µL/mL) and 10% 2X medium. After preparing this solution, thrombin is added (0.3% of total volume, 20U/mL). The whole solution is pipetted gently in the top channel, until all four chambers are filled up. After that, the solution in the top channel is pipetted out. When preparing just one chip, all the solution in the top channel is dead volume. When preparing more chips, the solution from the top channel can be re-used for the second chip. The chip with the filled chambers is left for 10 minutes to form the EHTs. Then the bottom and top channels are filled up with the desired medium. Figure 20 shows a schematic representation of the µEHTs.

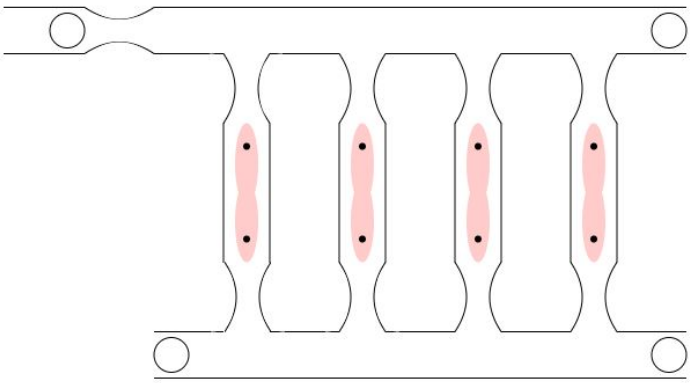

Figure 20: Schematic representation of the formed µEHTs (top view), with top and bottom channels and inlets/outlets indicated with the circles.

3.14 µEHT maintenance

Since the µEHTs have a different format, they cannot be refreshed by simply refreshing 1mL of medium out and 1mL of medium in. As stated above, the µEHTs are supplied with medium through the channels that are connected to the chambers which contain the actual tissues. The easiest way of refreshing the tissues is by pipette tip setup, figure 21 shows the pipette tip setup which was used in the experiments in this research. Two pipettes each containing 45µL of medium are put into the top and bottom left channels of the chip. Then two pipettes each containing around 200µL of medium are put into the top and bottom right channels of the chip. After this step, the medium will start flowing from the right side of the chip towards the left side of the chip, providing the EHTs with nutrients.

Although this is a very easy way of maintaining the tissues, it is desired that the tissues are

provided with a constant flow of nutrients, as this is more closely mimicking the *in vivo* situation of the heart. For this purpose, the Harvard apparatus syringe pump is a stable alternative to provide the desired flow in the µEHT chips. This will be explained further in the recommendations/future outlook section.

Figure 21: The µEHT chip with the pipette tip setup for tissue maintainance

3.15 µEHT experiments

The following experiments are carried out using the µEHT format:

- Testing of the µEHT platform with only fibrinogen
- Testing of the µEHT platform with CMs and FBs
- µEHT platform with CMs ECs and FBs

The testing of the µEHTs is done using only fibrinogen, matrigel, and thrombin to check if the matrix will form inside of the µEHT format and compacts around the PDMS posts. A mix of 60µL without cell solution is made and pipetted inside of the chip.

µEHTs were cultured in medium containing TDI, lactate, and low glucose (same concentrations as stated in section 3.3). The amount of CMs used in this experiment is approximately 400k per chip, with 3% of FBs (12k per chip). The purpose of this experiment is to test if the EHTs will form properly and survive the 10 days of culturing so their contraction can be measured.

For the experiments with EC co-culture, the COUP TF-II cell line is used. The lactate medium was supplemented with VEGF (50ng/mL) and SB50 (10µM). The amount of CMs used was 850k per chip, with 3% FBs (25.5k per chip). One experiment consisted of four different chips, with the following conditions: 0% ECs, 25% ECs, 50% ECs, and 75% ECs (with respect to the used CMs). The resulting total number of cells per EHT chamber per condition: 0%: 69k. 25%: 86k. 50%: 102k. 75%: 119k.

3.16 EHT and µEHT contraction force measurements

Contraction measurements were done at d10 of EHT/µEHT maturation. The tissues were paced and images were acquired by the Nikon Eclipse TE2000-U fluorescence microscope. Excited by mercury light images at 70 frames per second. After this, the images and videos of the tissues were analyzed by customized software. As discussed before, this software will track the black dots on the PDMS pillars and detect the tissue area. From this software, the following parameters are included in the analyses.

- **Absolute force** This is the absolute force generated by the tissue
- **Initial Load** Initial load or preload is the initial stretching of the CMs prior to contraction
- **Force per area** The force exerted per mm2 in µN/mm2
- **Contraction and relaxation speed** Speed of contraction and relaxation in m/s
- **Force contraction and relaxation speed** The amount of force the tissue exerts per second while contracting and relaxing in µN/s
- **Contraction and relaxation time 10 percent** The time it takes the tissue contract or relax the first 10% of the total distance covered during a contraction or relaxation
- **Contraction and relaxation time 90 percent** The time it takes the tissue contract or relax the first 90% of the total distance covered during a contraction or relaxation

Taking all these parameters into account, we can assess the contractile performance of the EHTs and µEHTs. The contraction measurements done in µEHT format required updating the analysis software.

3.17 Testing of the new thrombin

In almost all the experiments, standard batch thrombin is used for the gelation of the cells/mix mixture. The standard solution contains 20U of thrombin per mL. However, the new batch of thrombin is stronger, containing 100U/mL. With the standard solution, new thrombin was diluted in 0.1% BSA solution.

The new thrombin is tested based on the number of units used in the original protocol. However, it cannot be calculated towards the same amount of units because pipetted volumes are too small then and is not practical to use. The tested conditions are 1 well (3 tissues), 2 wells (6 tissues), 4 wells (12 tissues), and 6 wells (18 tissues). The test is carried out with only fibrinogen since this is the compound in the mix that is influenced the most by the thrombin. The projected gelation time is around 4-6 minutes from the moment that the thrombin is added to the fibrinogen. The solution is pipetted every minute, starting at t = 2 minutes. It can be quite challenging to point out the exact moment where the solution is gelated. This is done by pipetting and sometimes stirring the solution. When the solution cannot be pipetted anymore, it normally means it is gelated. Also, when it is totally gelated, you see a formed gel inside of the solution.

3.18 Statistical analysis

Statistical analyses of contraction measurements were performed in GraphPad prism. Using a two-tailed students t-test for comparing FLB and MYBPC3 measurements. The PE and

The µEHT experiments were statistically evaluated by a one-way ANOVA with Tukey multiple comparisons testing for comparing each group individually for the µEHTs and Dunnett's multiple comparisons test for the PE measurements. For every test: $p < 0.05$ (95% confidence interval) is considered statistically significant. Asterisks in figures: $p < 0.05$ = *, $p < 0.01$ = ** $p < 0.001$ = ***.

4 Results

This section of the report will show the results of the contraction measurements of the disease models generated with the non-purified CMs and the lactate purified CMs. We will cover the morphology of the tissues with images of the EHTS. Also, we will discuss the results of the PE-induced disease model. Furthermore, the formation of the µEHTs will be discussed together with the contraction measurements from the co-culture with ECs.

Also, we will discuss the results of the testing of the new thrombin. So the further experiments with the thrombin can rely on these results and will ensure optimal gelation times for the formation of future EHTs.

4.1 Regular EHT formation

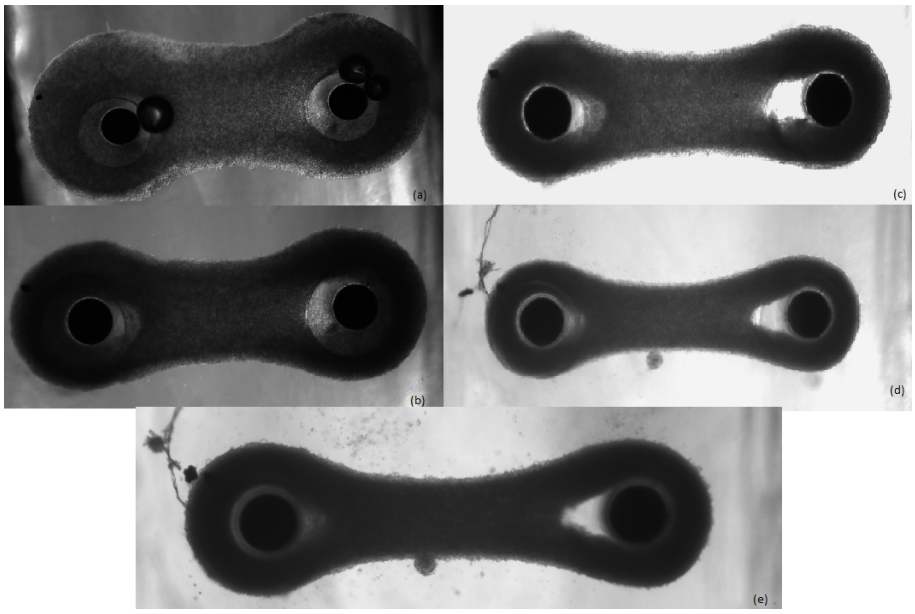

Figure 22: Formation of the regular EHTs (a) the EHT right after pipetting (b) day 2 (c) day 3 (d) day 8 (beating) (e) day 10

Figure 22 shows the formation of an EHT cultured with 800k FLB CMs and 40k cFBs (5%). The onset of beating is usually around d4. Light compaction can be seen d0 to d3. At d8, the tissue is completely compacted and beating very nicely.

4.2 FHCM HF model with HS supplemented culture and un-purified CMs

The following section will display the FHCM/HF model with un-purified CMs, the tissues are made and maintained in medium supplemented with 10% HS. We will discuss the contraction patterns and differences between the healthy cell line and the mutated cell line. All results in this section are contraction measurements done on d10 of EHT culture.

From direct observation, it was already clear that compared to the FLB tissues, the MYBPC3 tissues were contracting in a different rhythm and had a slightly twitchy contraction pattern. We observed that the MYBPC3 tissues were exerting less force on the pillars. Figure 23 shows that the absolute force of contraction is approximately 40µN compared to +- 120 µN for the FLB

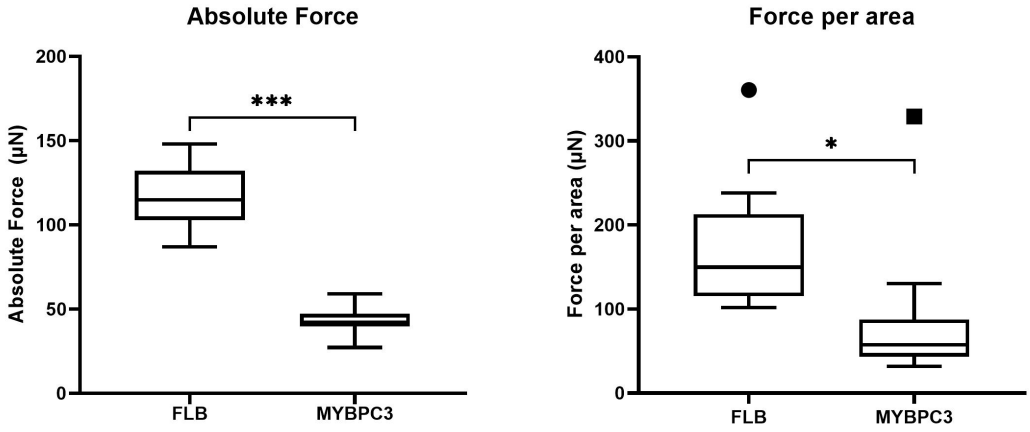

Figure 23: Absolute force of contraction and force per area of the FLB and MYBPC3 cell lines, *** p<0.001

tissues. Which is a very significant difference (p<0.001) and about a 3-fold decrease in absolute force. Figure 23 also shows force per area of the FLB and MYBPC3 tissues. There is a smaller difference in force per area in between the FLB and MYBPC3 tissues compared to the difference in absolute force, with a higher p value (P<0.05). The difference in force per area is expected to be comparable to the absolute force because the tissues have a comparable area that does not differ that much from each other (700-850mm2). The difference in significance with the absolute force and force per area can be explained by the fact that the detection software was having a hard time detecting tissue area which were oddly shaped due to variability in formation. This resulted in outliers because of the variability in tissue shape. This is where the µEHTs can provide a solution, which have a more regular way of formation and are less prone to handling errors.

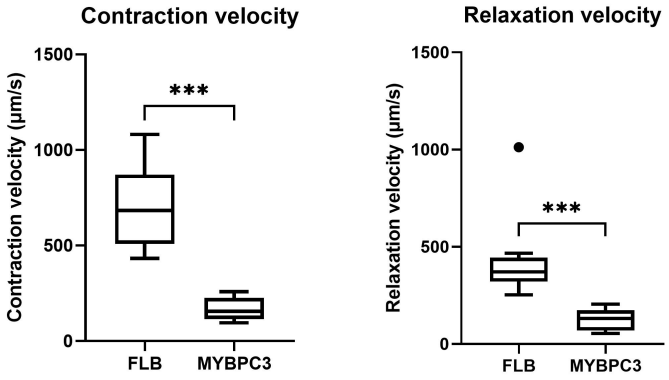

Figure 24: The contraction and relaxation velocities of the FLB and MYBPC3 cell lines *** p<0.001

Also, the contraction and relaxation velocities were significantly lower in the MYBPC3 tissues compared to the FLB tissues. We observed a 4-fold decrease for contraction velocity and a 3-fold decrease for relaxation velocity as can be seen in figure 24. This makes sense because the absolute force of contraction is higher, making the pillars move closer to each other, meaning that there is more distance covered. With the same frequency of pacing, it is logical that

the contraction speed is lower as well. This is an excellent example of the disease model that mimics a diseased and weakened tissue, which is also apparent from the absolute force.

Force contraction/relaxation velocities were also significantly lower in the MYBPC3 tissues compared to the FLB tissues. This can be found in the supplementary material in figure S4. This is consistent with what we observe in the contraction/relaxation velocity graph. We observe the same trend as in the previous graphs. Where the force contraction and relaxation velocities of the MYBPC3 cell line are significantly lower than the control cell line ($p<0.001$).

Contraction and relaxation times (10% and 90%) can be found in supplementary material (figures S2 and S3. In the window of the 10%, there is no significant difference to be seen between the FLB and MYBPC3 cell lines. The values are very close to each other. For the contraction and relaxation times 90%. There is a slight difference between the FLB and MYBPC3 cell lines. The MYBPC3 90% contraction and relaxation times are significantly higher ($p<0.01$ for TC90% and $p<0.05$ for TR90%). Indicating that the relaxation of the mutated cells takes slightly longer than the healthy control.

4.3 FHCM HF model using lactate purified CMs

The following section will show the results of the experiments done with lactate purified cells as well as the FACS analysis results. As described in the materials and methods section, we use three different batches of cells of the FLB and the MYBPC3 lines. First, we compare the three different batches of cells to see if there is a contractile difference. This comparison will cover absolute force and contraction, and relaxation speeds. Then, the contraction parameters of the FLB vs. MYBPC3 will be shown.

4.3.1 FACS analysis

Samples were analyzed with FACS to assess the lactate purification with a minimum of 100k cells/sample. Table 1 shows the FACS results. One immediately obvious thing is that the percentage of CMs in the FLB batch from June 22nd is low, and the content of CMs in the MYBPC line of June 22nd is relatively high. Also remarkable is that the CM content in the FLB line from June 7th is 86%, which is expected from a successful lactate purification. Also, the purification of the FLB line of May 9th performed relatively well with a CM yield of 67%. For the FACS analysis, we can conclude that the lactate purification performed poorly, where a CM yield of around 90% is desired and expected. Unfortunately, the % of CMs in the non-purified cells experiments were not measured. For better comparison, it would be desired to culture the same batch of cells and take a FACS sample of the non-purified cells.

Cell line	Batch	CM %
FLB batch 1	9-5-2020	67
FLB batch 2	7-6-2020	86
FLB batch 3	22-6-2020	38
MYBPC batch 1	9-5-2020	49
MYBPC batch 2	7-6-2020	50
MYBPC batch 3	22-6-2020	74

Table 1: Results of the FACS analysis for the different batches of FLB and MYBPC3 cells

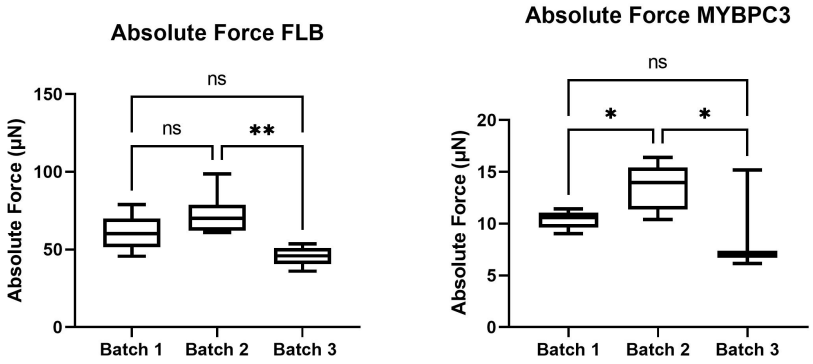

Figure 25: The absolute force of contraction of the different batches of FLB and MYBPC3 cells ** $p<0.01$ * $p<0.05$

Figure 25 shows that the absolute force exerted by the second batch of the FLB cells is the

highest and the third batch of FLB cells the lowest. This is in line with the FACS analysis, which points out that the second batch contains the highest percentage of CMs and the third batch the lowest. In the MYBPC3 batches, we do see the highest absolute force in the second batch, which is not in line with what is found in the FACS analysis.

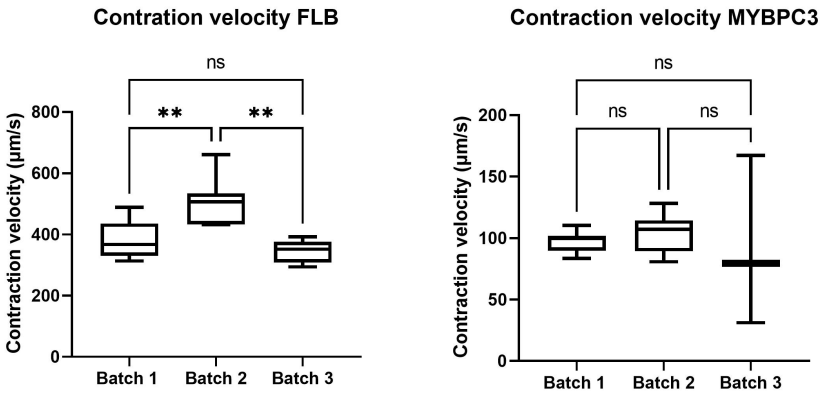

Figure 26: The contraction velocities of the different batches of FLB and MYBPC3 cells ** $p<0.01$

Figure 26 shows the contraction velocities, the same pattern as the absolute force is observed in the FLB batches. In the MYBPC batches, there are no significant differences in contraction velocities.

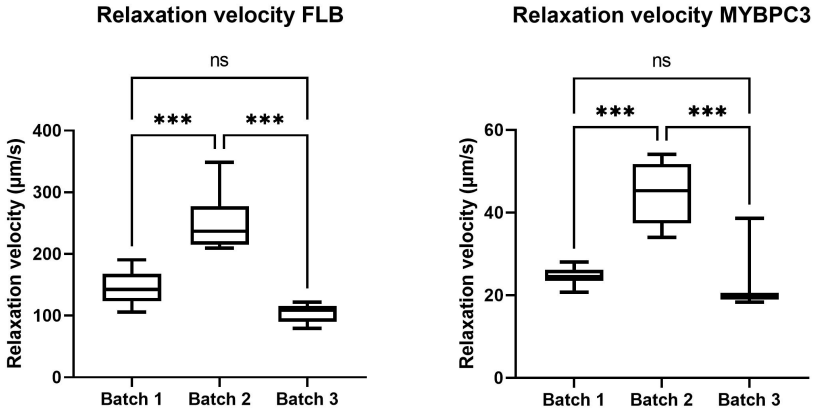

Figure 27: The relaxation velocities of the different FLB and MYBPC3 cell batches *** $p<0.001$

In terms of relaxation velocity shown in figure 27, we see the same pattern in the FLB cell lines as mentioned above. In the relaxation velocities of the MYBPC3 cell batches, we can see a significant increase in relaxation velocity in the second batch of cells $P<0.001$, compared to the other two batches.

4.3.2 FHCM model contraction measurements

The following section will show the results of the contraction measurements of the FLB and MYBPC3 lactate treated cell lines. Compared to the previously discussed disease model, the lactate purified EHTs are cultured in medium containing lactate and low glucose (without HS). The differences in contraction between the two cell lines will be discussed here. The total data points generated of the FLB cell line is 21 (9 for batch 1, 7 for batch 2, and 5 for batch 3). For the MYBPC3 cell line, the total data points is 21 (9 for batch 1, 9 for batch 2, and 3 for batch 3).

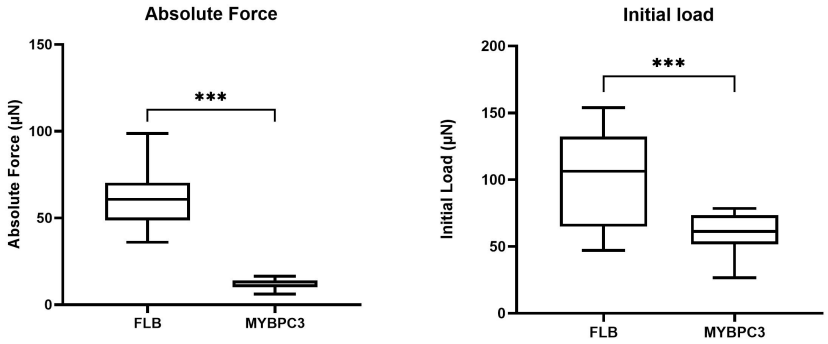

Figure 28: The absolute force and initial load of the lactate purified FLB and MYBPC3 cell lines *** $p<0.001$

From direct observation it was clear that the FLB tissues exerted more absolute force than the MYBPC3 tissues. This was also seen in the experiments with the un-purified CMs and can be seen in figure 28. Where it is visible that the FLB cell line exerts significantly more absolute force (6-fold increase) than the MYBPC3 cell line ($p<0.001$), which is expected for those two cell lines, and also in line with what is found in the non-purified FHCM model. Figure 28 shows the initial load of the two cell lines. Again, the initial load of the mutated cells is significantly lower than the healthy control ($P<0.001$). This is in line with the expectation and the previous result in absolute force.

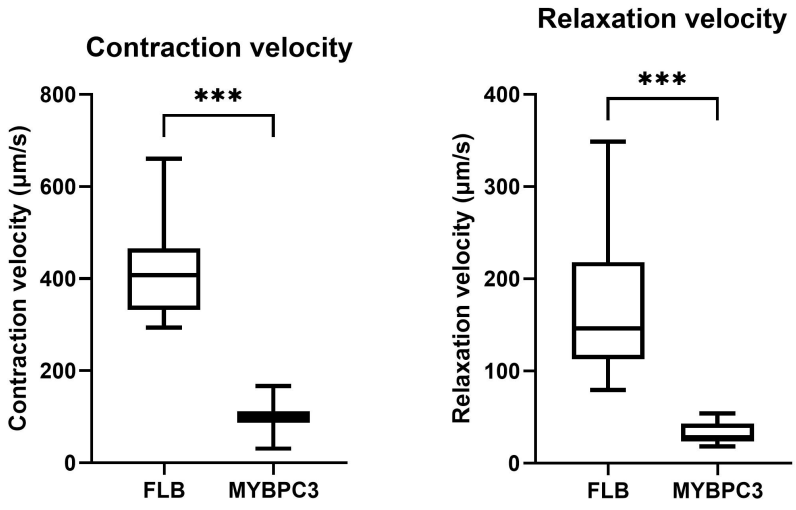

Figure 29: The contraction and relaxation velocities of the lactate purified FLB and MYBPC3 cell lines *** $P<0.001$

Contraction and relaxation velocities observed in the MYBPC3 tissues were significantly lower compared to the FLB cell line ($P<0.001$) as can be seen in figure 29. This is in line with the lower initial load and absolute force, and also consistent with the data obtained from the non-purified FHCM model.

Force contraction and relaxation velocities were significantly lower in the MYBPC3 tissues compared to the FLB tissues. This is shown in the supplementary material (figure S5). Again, we see a significant increase in force contraction and relaxation velocity in the FLB tissues. This is consistent with what is found and discussed above.

Contraction and relaxation times 10% and 90% can be found in the supplementary material (Figures S6 and S7). We find significant differences in contraction times between both cell lines ($P<0.001$), where the contraction times in the FLB tissues are higher than the MYBPC3 tissues. The trend can be seen for the relaxation times. Where also the FLB tissues have higher relaxation times than the MYBPC3 tissues. The difference in TR10% is slightly higher than the difference in TR90%. Something to note, the results of these contraction times are inconsistent with what we found in our non-purified CM HF model. Where the TC and TR 10% had no significant difference between the cell lines and the TR and TC 90 % were significantly elevated in the mutated EHTs compared to the healthy control.

Comparing these results to the absolute force and contraction and relaxation velocities found in the un-purified cells. We observe that the purified cells overall exert less absolute force and have a lower contraction relaxation velocity. This will be elaborated on in the discussion section.

4.4 PE FHCM HF Model

The following section will show the experiments for the disease model with the healthy FLB cell line treated with PE for inducing cardiac hypertrophy, assessed by contraction force analysis.

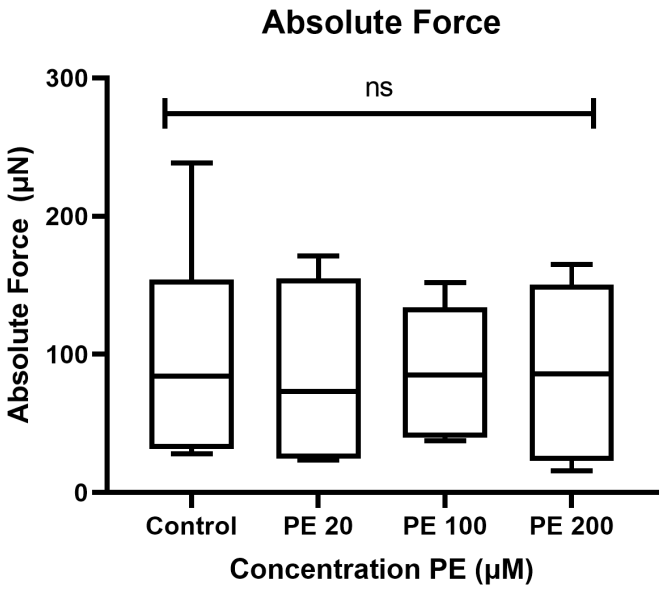

Figure 30: Absolute force of the tissues treated with different concentrations of PE, no significant differences were observed

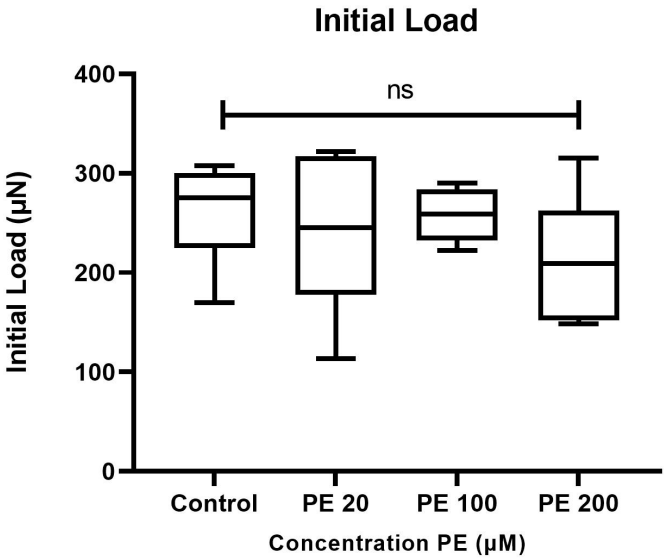

Figure 31: Initial load of the tissues treated with different concentrations of PE, no significant differences were observed

Absolute force exerted by the tissues is roughly the same for every concentration of PE after adding it to the wells for seven days in a row. The same is true for the initial load, as can be seen in the figures 30 and 31. This means that the PE does not influence either the absolute force or the initial load. The only thing that is visible is a slightly lower initial load for the the

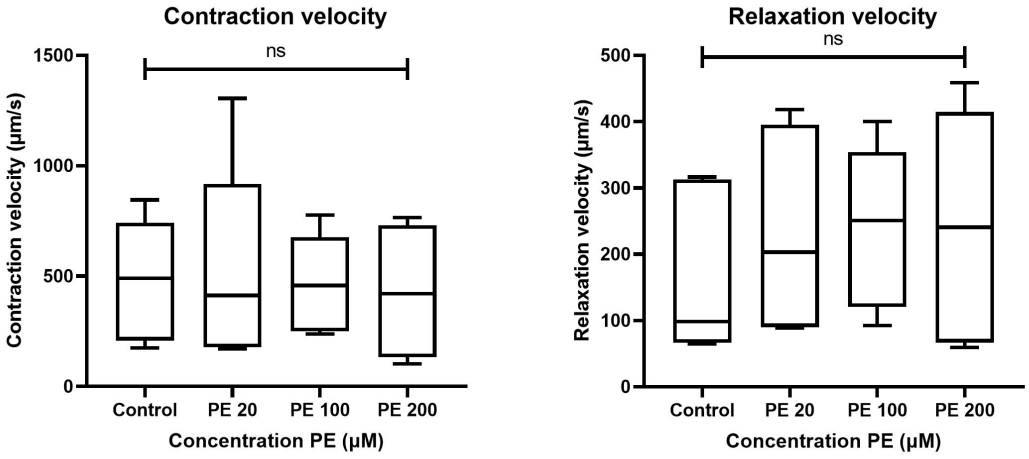

Figure 32: The contraction and relaxation velocities of tissues treated with different concentrations of PE, no significant differences were observed

tissues with 200 µM PE, but there is no significant difference observed between the control group and any of the groups with different concentrations of PE.

Contraction and relaxation velocities were also not influenced by the PE as can be seen in figure 32. Again, there is no significant difference between the control group and PE-treated groups. The only visible trend is that the relaxation velocity appears to increase slightly the higher the concentration of PE is. Overall, there is no significant difference observed in any of the contraction parameters under the influence of PE. Meaning PE has no effect on the contractile parameters of the EHTs in this format.

4.5 µEHT results

In this subsection, the results of the µEHTs will be discussed. This includes the testing of the µEHT format with only fibrinogen, which will be evaluated with pictures. Also, we will discuss the formation of the µEHTs with only CMs and with CMs with FBs to see if they can form properly while using fewer cells. Last, we will look at the formation of the with different percentages of ECs. With these tissues, contraction analysis is also included to see how the tissues perform contraction-wise under these different conditions.

4.5.1 µEHT formation

Figure 33 shows the formation of the µEHTs evaluated in one chip. Within each chip, the fibrin base where normally the CMs are present is clearly visible in each chamber. Also, there is still some space between the fibrin scaffold and the wall of the chip, meaning that the fibrin does not adhere to the surface. Also, every scaffold is formed nicely and without bubbles, except for chamber (c), where the bubble is present on the bottom right corner of the chamber. This emphasizes the importance of careful pipetting, because bubbles can disrupt the formation of the actual tissues.

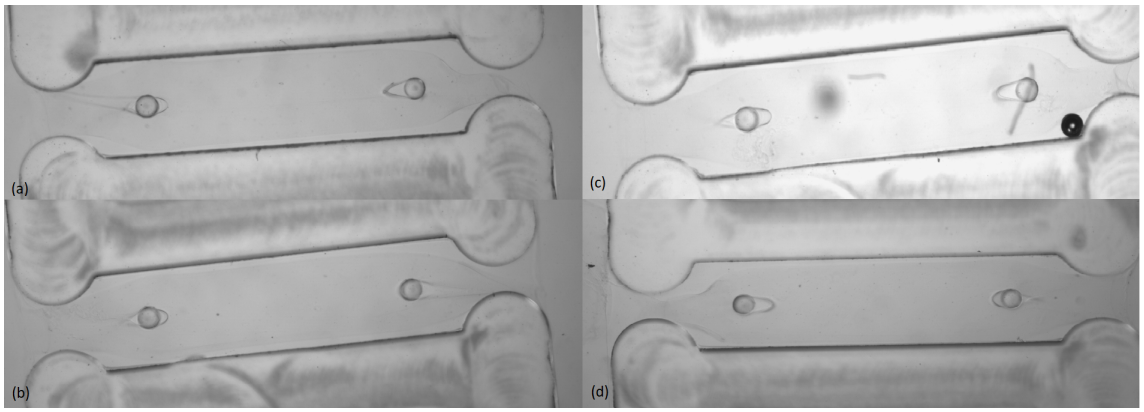

Figure 33: Formation of µEHTs using only fibrinogen (a,b,c,d) chamber (1,2,3,4) (c) shows a chamber with a bubble in the bottom right corner

4.5.2 µEHT formation using only CMs

This subsection will show the µEHTs formed with only CMs. Unfortunately, contraction analysis was not possible due to tissues detaching from the pillars, which in their turn is probably due to the low amount of cells used in these experiments (+- 400k/chip). Because of that, the structure of the tissues and formation will be discussed using pictures in various stages of the formation.

The results from the formation experiment with only CMs can be seen in figure 34. The compacted tissues on day 3 can clearly be seen. On day 6 (over the weekend), the tissue has detached from one of the pillars (figure 34d). The onset of beating occurs on day 3. The detachment is directly linked to the onset of the beating. The beating makes the pillars on the inside move, creating a small space between the bottom of the chip and the bottom of the pillar. In this format, the tissues do not have enough cells to cling tight enough to the pillars. The detachment of the tissues does not impair tissue beating, as they are still beating after detachment. However, contraction analysis cannot be done with detached tissues because there is

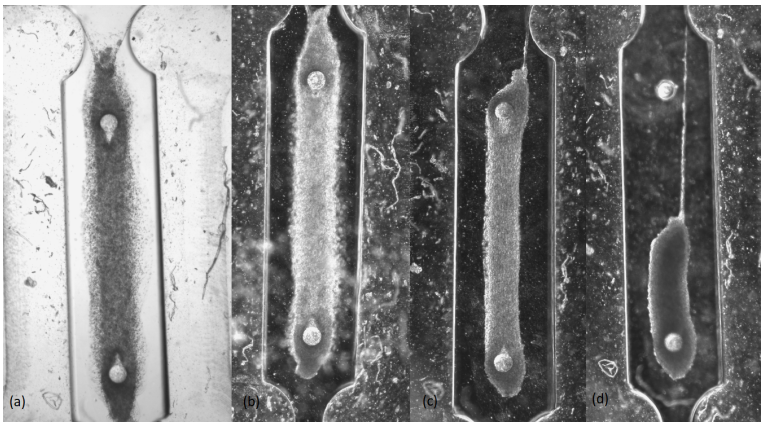

Figure 34: The formation of the µEHTs using only CMs. (a) is the tissue on day 1, (b) is the tissue on day 2, (c) on day 3, and (d) on day 6

no specified beating area, making them unusable for further experimenting. The formation of the other µEHT chip can be found in the supplementary information (figure S8). In both chips, strings of CMs that are connected to the outside of the chamber are still visible.

4.5.3 µEHT formation using CMs, cFBs and cECs

This section will show the experiments conducted with µEHTs combined with CMs, FBs, and ECs. The formation will be discussed, as well as their contraction patterns. The µEHTs were cultured with the COUP TF-II CM cell line. The differences in contraction between the tissues with the different percentages of ECs will be discussed, leading to a conclusion on the influence of ECs on the microtissues.

4.5.4 Results formation of tissues using ECs

We will first discuss the formation using pictures. As can be read in the materials and methods section, we will evaluate the formation of tissues with 850k CMs, 0%, 25%, 50%, and 75% of ECs and 3% FBs for all conditions. Following the results of the tissues with only CMs, it was clear that the cell density of the tissues was too low causing the tissues to detach.

Figure 35 shows the formation of the µEHTs with 0% ECs an 3% FBs. It is clearly visible that on the first day, almost all of the well is filled up with a dense layer of cells. On day 2, they already have compacted well and on day 5 they are completely compacted and beating. The tissue is not uniform everywhere and the observed beating appeared irregular. The CMs did not contract simultaneously, creating a contraction pattern that looked like a wave.

Figure 36 shows the results of the tissues with 25% ECs and 3% FBs. Right after seeding, the cells and matrix are almost filling the whole of the chamber. On day 2, the tissue has already compacted. The same can be seen on day 5, where the tissue has formed into a very clean and solid EHT. The onset of beating is around day 4. Also, these tissues all survived until day 10. Overall, these tissues have a slightly cleaner look than the 0% tissues. And appear to have a smoother area around the edges. Also, the beating pattern of these tissues was smoother than the 0% tissues. Where the beating was observed to be more regular.

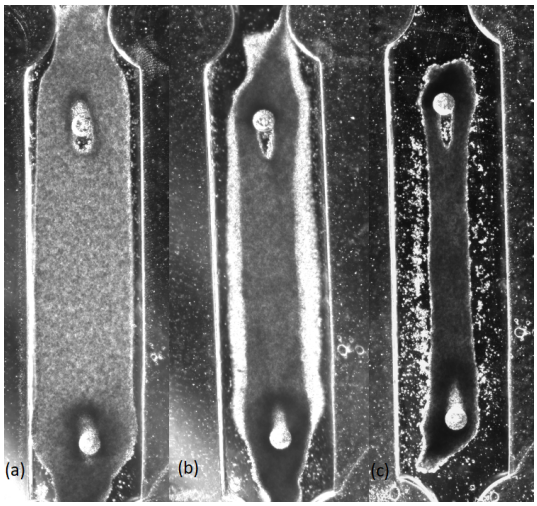

Figure 35: Formation of the µEHTs with 0% ECs (a) tissue on day 1 (b) tissue on day 2 (c) tissue on day 5

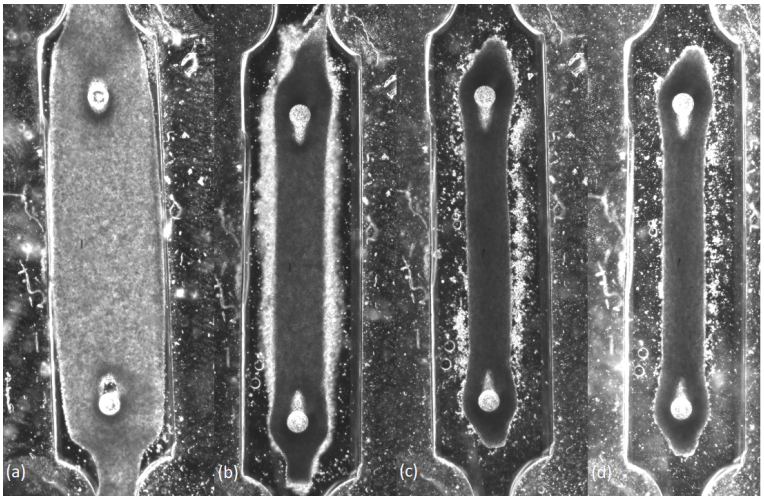

Figure 36: Formation of the µEHTs with 25% ECs (a) tissue on day 1 (b) tissue on day 2 (c) tissue on day 5 (d) tissue on day 6

Figure 37 shows the tissue formation with 50% ECs and 3% FBs. It is clear that there are more cells involved, right after seeding the chamber is filled up with cells, which also compacts very well at day 2. On day 5, like with the 25%, the compaction appears to be done and there is an onset of beating. Also, you can see the strings of CMs being present in the top of the chamber on day 1 and 2. After compaction is complete and beating is starting, these strings appear to be disappearing and snapping. These tissues also made it to day 10 without any problems. From first look, contraction-wise and formation-wise, the tissues are very comparable with the 25% EC tissues.

Figure 38 shows the formation of the tissues with 75% ECs, the formation is almost the same as with the 50%. The onset of beating is also at day 4/5. Also, a big portion of these tissues did not make it to D10, some of them detached, and some of them were unable to be analyzed.

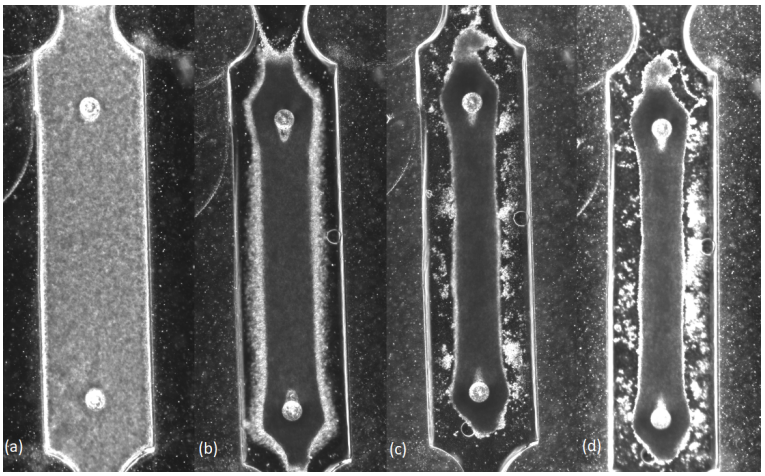

Figure 37: Formation of the µEHTs with 50% ECs (a) tissue on day 1 (b) tissue on day 2 (c) tissue on day 5 (d) tissue on day 6

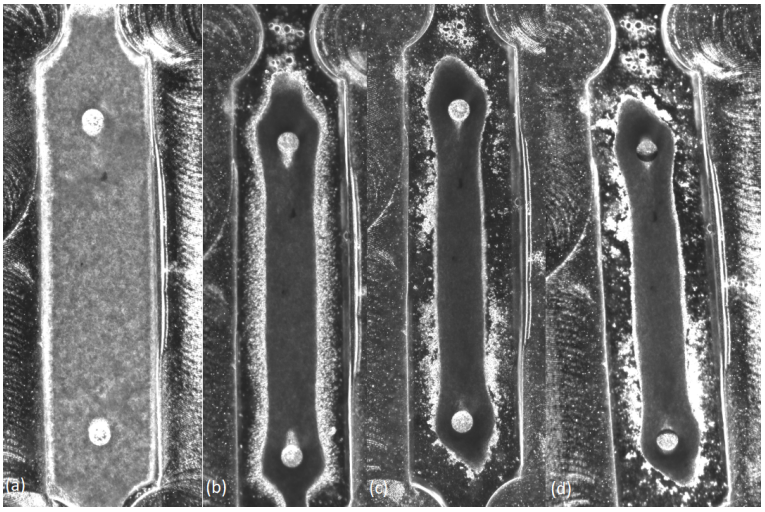

Figure 38: Formation of the µEHTs with 75% ECs (a) tissue on day 1 (b) tissue on day 2 (c) tissue on day 5 (d) tissue on day 6

During formation, the following problem was observed with some of the tissues. Clumps of CMs could potentially block the entrance to the chamber. A picture of this can be found in the supplementary material (figure S9). It is visible that this clump is sticking to the side and connected to the tissues, also potentially influencing the contraction pattern of the tissue. It is currently impossible to remove this clump as it is deep inside the chip and we are unable to reach this part of the chip. Although this is hard to verify, this blockage will cause a reduced flow of medium in this chamber and will disrupt the nutrient flow to the tissue.

4.6 µEHT contraction measurements

As can be read in the materials and methods section, we will primarily look at absolute force of contraction and force per area of the tissues, as well as contraction and relaxation speeds. This analysis is based on the tissues that the measurement software was able to detect and the tissues that survived. For the 0% tissues that number is 5, for the 25% it is 9, 50% it is 11 and another 5 for the 75%. We can also say that the formation of the 25/50% tissues is the most stable and these tissues make it to day 10 on most occasions.

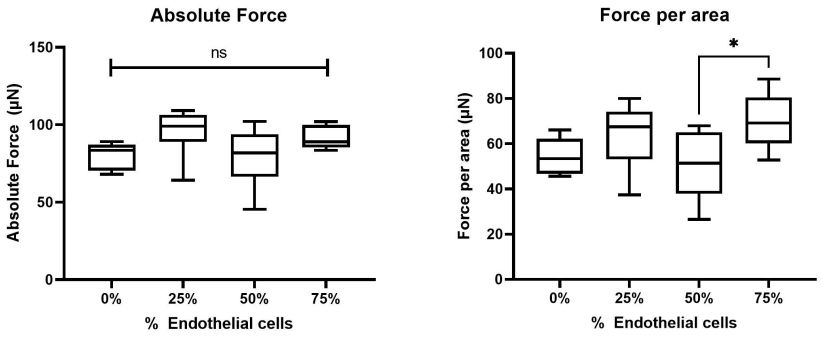

Figure 39: Absolute force and force per area of the tissues with different percentages of ECs

The tissues with 25% and 75% ECs exert slightly higher absolute force than the tissues with 0% and 50% ECs. And the 25% was exerting the most absolute force. This can be seen in figure 39. However, these differences were found to be non-significant by one-way ANOVA. For the force per area the same trend is visible, the 75% tissues exert the most force per tissue area as can be seen in figure 39, where we would expect less force per area due to more cells (= more tissues area) and less cells being CMs. This could indicate that the ECs in their highest percentage have a stimulating effect on the contraction force of the tissues. Also the force per area in the 25% tissues is slightly higher than the 0 and 50 %. The only significant difference found is that between the 50% and 75% ECs with ($p<0.05$).

Contraction and relaxation velocities were not influenced by the percentage of ECs present in the tissues as can be seen in figure 40. The only visible thing is that the mean contraction

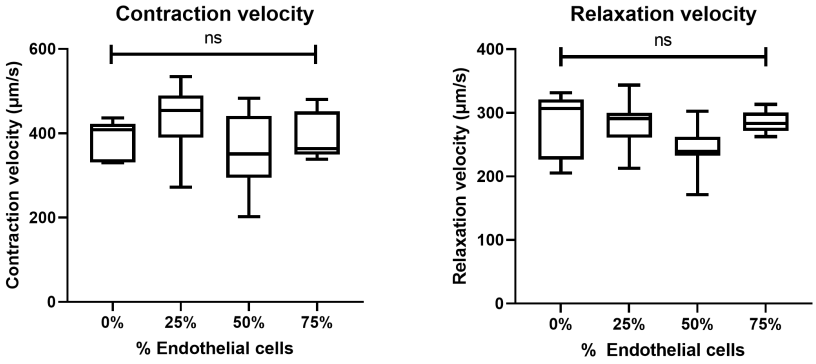

Figure 40: The contraction and relaxation velocities of the tissues with the different percentages of ECs

velocity of the tissues with 50% ECs have a slightly lower contraction and relaxation velocity. But overall, the contraction and relaxation velocities are comparable and there is no significant difference to be observed.

Force contraction and relaxation velocities can be found in the supplementary information (figure S10). For the relaxation velocity, there is no significant difference between the tissues with different percentages of ECs. For the force contraction velocity, the only significant difference found is between the 25 and 50% tissues with $p<0.01$.

Contraction and relaxation times can be found in the supplementary information (figures S11 and S12). TC 10% are quite comparable and have no significant differences. For the TC 90%, we observe slightly elevated contraction times the more ECs are present in the tissue. The difference between the 0% and 75% is found to be statistically significant. This can be explained by the fact that the tissues are somewhat stiffer and there is more cell-cell communication going on, and differences in this cell-cell communication can produce different contraction patterns [86]. In the end, the ECs appear to have a small effect on the contraction times, with those contraction times being higher for the TC90%. The difference between the 0% and the 75% is the only significant difference.

For the relaxation times of the tissues a slightly different trend was observed. TR10% is slightly increasing with the presence of ECs. With the 25% and the 50% almost the same and 75% having a slightly higher TR10%. The only significant difference is that of the 0% vs the 75%. We see an increase in TR 90% in the tissues containing ECs, regardless of the percentage that is present, although this difference is not found to be significant with p=0.5. Indicating that merely the presence of ECs has an impact on the relaxation time of the tissues, but the number of ECs does not affect it.

4.7 Testing of the new thrombin

Table 2 shows the results of the tested thrombin. As discussed in the materials and methods section, the optimal gelation time of the mixture is 4-5 minutes. For the experiments with the fibrinogen for the 1,4 and 6 wells, the optimal amount of thrombin for an optimal gelation time is pretty well defined and can be found in the table. For the two well experiment, the gelation time was around 3 minutes for the 0,86 µL of diluted thrombin. This was when the first gelation was visible, and the whole solution was still pipettable for up to 7 minutes.

Amount of wells	Tissues	Fibrinogen (µL)	Thrombin (µL) 20U/mL	Units Thrombin	Gellation time
1	3	4,9	0,23	0,0046	>8min
1	3	4,9	0,45	0,009	4-5 min*
1	3	4,9	0,68	0,0136	1-2 min
2	6	9,4	0,86	0,0172	3 min**
2	6	9,4	1,3	0,026	2.5 min
4	12	18,4	0,85	0,017	5-6 min
4	12	18,4	1,28	0,0256	5 min
4	12	18,4	1,69	0,0338	4 min***
6	18	27,4	1,26	0,0252	>7min
6	18	27,4	1,89	0,0378	4-5 min
6	18	27,4	2,52	0,0504	3-4 min

Table 2: Gellation times of different volumes of fibrinogen with different volumes of thrombin.* First gellation (string) visible after 3 minutes ** After 3 minutes it appeared to be gellated and was hard to pipette, but the whole mixture was still pipettable up to 7 minutes *** Hard to pipette after 2 minutes

5 Discussion

In this study, we developed a disease model for FHCM using hiPSC derived EHTs to see if we could model the contractile deficits expected in a CM cell line carrying a MYBPC3 mutation. Where models in the past used similar cell lines [11] in a 2D format, and many animal models with cMYBPC3 deficiency have been studied [16, 17]. An *in vitro* model of patient-derived hIPSCs with an induced mutation in the MYBPC3 gene in EHTs was lacking. We assessed the contractile performance of both our healthy control and the MYBPC3 mutated disease model. The contractile deficits observed in our model are mostly significant and show a decrease in contraction force and speed of contraction in disease models using either non-purified or lactate purified CMs. These contractile deficits were already (partly) researched in previous studies using hIPSCs derived 2D models [11, 82], where a contractile deficit was also observed. Similar results were observed in mouse models, where maximal force of contraction is reduced by +- 40% in mice carrying a MYBPC3 mutation [87]. Wijnker et al. [18] reported on the use of EHTs with MYBPC3 KO-Mice cardiac cells. They reported an increase in contraction force compared to the WT EHTs. Which is in contradiction with our findings. They also did not find a significant difference in contraction kinetics, also in contradiction with our findings. An important difference is that we make use of hiPSCs EHTs, which can be an indication of a better performing 3D model to unveil the contractile characteristics of FHCM. Also, they studied different MYBPC3 mutations ((c.2373-2374insG) and (c.1591G>C)). Which is most likely the reason for the different pathological effect that is observed. This makes studying further mutations of the MYBPC3 gene an interesting outlook for our hiPSC derived EHTs. Van Dijk et al. [5] showed decreased force of contraction in 2D cultures from cardiac biopsies with the c.2373dupG mutation. Where our model in the EHT format showed a more apparent decrease of contraction force. Consistent with the hypothesis that the MYBPC3 mutation causes contractility deficiencies, and these contractility deficiencies are more visible in EHT format [61]. Also, Van Dijk et al. used primary cells from patients carrying the mutation, which can mean that the onset of hypertrophy or HF was not yet visible in the phenotype.

Right now, most of the HCM models using MYBPC3 mutation/deficits rely on single-cell analyses or 2D monolayer cultures, 3D models have also been reported. Ma et al. [83] reported on a 3D model of HCM using cardiac microtissues in fibers which compared contractile function between WT hiPSC CMs and MYBPC3 deficient hiPSC CMs that totally lacked MYBPC3 expression. They reported slightly lower maximal forces and higher contraction velocities in the MYBPC3 deficient microtissues. Where our differences were and velocities observed were lower in the MYBPC3 tissues.

However we were able to show a significant contractile difference in EHTs in the MYBPC3 mutated hIPSCs, we cannot say for sure that this is an effect of hypertrophy or onset of HF because our analysis is based on contractile parameters alone. The underlying cause for the contractile deficit we observe in both models is unknown. For a complete understanding of the behavior of hiPSC-CM EHTs with the mutation in the MYBPC3 gene, like the presence of truncated MyBP-C and possible disruption of cellular alignment [8], more parameters should be taken into account. For testing the onset of hypertrophy in the cells, it would very valuable to be able to check cell size and tissue size, like done in [30] and [31], where they also assessed various hiPSC CM models with different MyBPC-3 related mutation based on cell size increase. These studies showed an increase in cell size in their hiPSC-CM models. But also Ca2+ sensitivity and electrophysiological properties would be interesting to look at, like done in [88, 89].

Research by Dambrot et al. [36] shows that the use of HS in CM cultures can mask the hypertrophic effects that are studied. Making the experiments of our FHCM model which make use of the HS-supplemented medium less reliable, because the effects of hypertrophy can be (partly) induced by the HS [36]. Given that the contraction force is higher in both FLB and MYBPC3 in the experiments with serum (un-purified) compared to the experiments without serum (purified) (about 2 fold), we can contribute this to the presence of HS and/or an effect of the lactate purification, because the serum can induce hypertrophy and on its own will increase functional output in CMs. [90, 91] Also, the batches used in the lactate purified experiments had a poor quality of differentiation, which also is a contribution to the difference in contraction force compared to the non-purified cells.

In the PE experiments, there are no significant differences found between the cells that were treated with PE and the control cells. Also no concentration dependent differences were observed. Something to note with these experiments is that the quality of the cells appeared to differ much between the two batches of cells the data was generated from. Meaning that the contraction forces and velocities differed between those batches. This could also be seen by eye, where the first batch of EHTs was beating very nicely, and the second were not. For the mean measured values of these experiments, this does not affect the general trend very much, but it needs to be considered here, as it could be an influence on the outcome. Foldes et al. [92] reported that hiPSC-CMs can be unresponsive to PE administration, whereas hESCs can be a better candidate for PE-induced hypertrophy. This is consistent with our result in terms of contraction parameters, and can be a reason to work with hESCs in a future FHCM disease model using PE as a stimulant for influencing contractile parameters in EHTs. Stenzig et al. [93] also treated tissues with PE to see the hypertrophic effects similarly, with 20µM of PE with seven days of stimulation, using CMs from neonatal rats. They did not find any significant differences in contraction force between EHTs and PE-EHTs as well. A similar way of PE stimulation is observed in the research of Friedrich et al. [94] where a decrease in contraction force and velocity is observed after treatment with PE, using neonatal rat CMs. A similar response would be expected in our PE experiments, which can also be explained by the fact mentioned above that hIPSCs appear to be unresponsive against PE [92].

Furthermore, this work showed a new method of EHT generation where EHTs are generated on microfluidic chips, which have the advantage of being easier to handle, use a lower amount of cells and therefore are cheaper to produce, and have the possibility of introduction of a constant medium flow. Jackman et al. [68] showed increased CM maturation in dynamic engineered myocardium cultures. Our cultures, although only evaluated with contractile measurements and formation pictures, had a higher survival rate until the day of measurement and a more regular way of forming, which will most likely improve the throughput and reliability of future results. Vollert et al. [64] stated that constant perfusion of EHTs improved cell density and tissue homogeneity, making use of vascularized microtissues with ECs.

Fabrication of EHTs and µEHTs

This study used a unique method of EHT generation in a 12 well format using PDMS pillars as shown in the introduction section. The pillars have shown to be able to hold three viable EHTs per well. However, the generation of the chips is still a time-consuming process that requires multiple steps and is still very prone to error. Over and underpainting of the pillars

is still a problem because under painted pillars are unable to be analyzed by the contraction measurement software. The fabrication of the plates is also a point of discussion. Besides from being time-consuming (mostly due to the alignment of the pillars) it still fails many times due to plates not sticking to the pillars, still being misaligned, and forming crooked. All this taken into account, of the projected 30 pillars from one mold, around 50 % ultimately makes it into the well plate. Considering this time-consuming method, its an outcome that is way too low and after all a waste of material (PDMS). To minimize the waste of pillars, the software could be upgraded to a system where it is able to track the tissues without the use of black dots. This would not only speed up the fabrication process, but also decrease the loss of pillars due to over or underpainting. Also, this makes the process of plating easier, because the painted pillars can lead to height differences between the pillars, which is increasing the chances of crooked plates. A disadvantage of this approach is that the tissues need to form uniformly and perfectly to be able to be tracked, past experience confirms that this is not always the case, leading to a loss of data due to undetectable tissues.

Considering the fabrication of the µEHTs. The process of making chips is easier and takes up less time. Also, no well plate preparation is necessary and ultimately takes less materials. Making this method of EHT generation excellent for increasing the throughput of the experiments.

A limitation in using the µEHT formation in the current form is that while pipetting in the cell solution, and thereafter sucking up the solution from the upper channel, sometimes one of the four chambers is emptied out as well. The problem here lies with the resistance in the upper left corner. When pipetting the solution, it should not go past that resistance. This requires very careful pipetting and close monitoring of the flow of the solution. A possible solution to the problem is to make the resistance smaller, so it easier to pipette the cell solution in without going past the top left resistance. This will result in less tissue loss and make it easier fill up all four chambers of the chip correctly.

6 Conclusions

We were able to show significant contractile differences in either lactate purified and non-purified hiPSC-CM EHT FHCM disease models, where other researchers showed differences in contraction that were smaller and less obvious, arguably due to the limitations of 2D culture. Making our EHT-based model excellent for comparing contractile parameters for disease modeling and future patient-specific drug testing and understanding of the complex mechanisms of FHCM.

Although PE is a known substance to induce hypertrophy in CMs [79, 80, 81], our contraction measurements did not indicate any statistically significant difference in either contraction force and contraction velocity. Meaning that the PE did not have an influence on our assessed contractile parameters. This does not mean it cannot induce hypertrophy or HF on EHTs, but more research needs to be conducted on that. But we could not model/show contractile deficits or HF by stimulation with PE alone.

Furthermore, we succeeded in culturing EHTs in a microfluidic chip that requires fewer cells, makes EHT generation easier, and increases the chances of tissue survival up to d10 of culture. The µEHTs give the option of dynamic culture with medium flow, which can have a positive

impact on the tissues, but more research is needed to evaluate that, as we did not incorporate fluid flow yet. Co-culture with ECs has a positive effect on the formation and survival of the tissues, but does not change the contractile characteristics significantly. More research needs to be conducted, like analyses of morphology, sarcomeric organization, and gene expression associated with CM maturation, like done in [86]. This can shine a light on the effects of co-culture with ECs and possibly other cells from the cardiac microenvironment in EHTs or µEHTs.

7 Future outlook/recommendations

Our FHCM model shows a significant decrease in contractile parameters in experiments with purified and un-purified cells. This gives insight into the way that the MYBPC3 mutation is changing the contractile parameters of the healthy cells. However, we cannot say that the contractile deficit is due to hypertrophic cells inside of the EHT format. For that, additional research has to be done to be able to show if the cells indeed became hypertrophic, or that a different process is causing the contractile deficit. Interesting parameters that can be studied are cell size, sarcomeric organization, Ca2+ sensitivity, gene expression, protein content, etc [74]. This will help us better understand the underlying mechanisms of FHCM, and can give a potential explanation for the contractile deficits observed. It can also give us insight in the maturity of the hiPSC-CM EHTs.

Overall, we produced a model that gave us new insights in the pathophysiology of FHCM. This method of disease modeling could potentially be used for the modeling of other (genetic) heart diseases by inducing other types of genetic mutations in the hIPSC CMs. Like Long QT syndrome or DCM.

We were not able to show the effects of contractile parameters for the stimulation of the EHTs with PE. There are multiple compounds used for hypertrophic stimulation, like angiotensin II. Foldes et al. [79] showed an increase of cell size in hESC CMs after stimulation with angiotensin II. Also, a commonly used compound is isoproterenol, for example, used in [92, 95]. Another commonly used compound for inducing pathological hypertrophy is endothelin-1 [54]. These can be interesting substances to induce hypertrophy in our EHTs in the future. Furthermore, as mentioned above, we do not know if the cells became hypertrophic, because the analysis is based on the contraction parameters alone.

We succeeded in making smaller EHTs with fewer cells. Future experiments of HCM HF models can potentially be done in the µEHT format to increase throughput. However, the amount of cells used does not decrease drastically (800k for 3 tissues vs 850k for 4 tissues). There is a new chip being developed where tissues can be formed in an even smaller format, these chips are developed by Tom Boonen and can potentially form tissues by using only 2k CMs per tissue. The supplementary material contains a picture of the mold used for generating these tissues (Figure S13). When those tissues can be made viable and feasible, many engineered heart tissues can be made with only one million cells, so cell number is less of a limitation and throughput will be increased.

Furthermore, in future experiments modeling FHCM with EHTs. The µEHT format could be used to make the disease model. This can also be combined by using co-culture of ECs together with the healthy cell line and the mutated cell line. Making a disease model that will

potentially more closely mimic the *in vivo* situation and potentially improve the results and throughput of the reported disease model.

The possibility of on chip EHT generation and co culture with ECs also gives rise to potential new EHTs. Where microfluidic EHTs could be cultured with ECs seeded inside of the microchannels to potentially create vascularized EHT, which will make the tissues more biomimetic and can hold promises for further disease modeling and drug testing [96, 97]. Moving us further towards a model that is mimicking the *in vivo* environment as closely as possible. These more biomimetic models could not only help modeling of cardiac diseases with hiPSCs, but also with ESCs.

The µEHT setup that is used in this research is a pipette tip static set up that has to be refreshed daily, which is explained in section 3.14. This setup needs daily refreshment to make sure the cells receive enough nutrients and is also static, which is not mimicking the *in vivo* situation. For future experiments, the use of dynamic refreshment will be a better way of providing the cells with a constant flow of nutrients while also mimicking the *in vivo* environment. The setup with flow could be realized with the use of a syringe pump.

8 Acknowledgements

At first, i want to acknowledge Dr. Marcelo Ribeiro for being my daily supervisor and helping me with the experiments throughout this research. I also want to acknowledge Beatriz Gamelas for being my project buddy, together we generated a lot of valuable data that set the basis of the disease models. I also want to thank Prof. dr. Robert Passier for his input and feedback towards finishing my thesis. Furthermore, I want to thank José Arbelaez MSc. for making the molds and helping me generate the chips. For the work with the µEHTs, I want to thank ir. Tom Boonen for the use of his molds and the support while making the chips and tissues and Carla Cofino MSc. for our discussions on the experimental procedures of the µEHTs. I also want to thank Dr. Ir. Jeroen Rouwkema for being the external supervisor at my colloquium. At last, I want to thank the students and members of the AST group.

References

[1] Familial hypertrophic cardiomyopathy — Genetic and Rare Diseases Information Center (GARD) – an NCATS Program.

[2] Hypertrophic cardiomyopathy - Symptoms and causes - Mayo Clinic.

[3] Ali J. Marian and Eugene Braunwald. Hypertrophic cardiomyopathy: Genetics, pathogenesis, clinical manifestations, diagnosis, and therapy. *Circulation Research*, 121(7):749–770, sep 2017.

[4] Christopher N. Toepfer, Hiroko Wakimoto, Amanda C. Garfinkel, Barbara McDonough, Dan Liao, Jianming Jiang, Angela C. Tai, Joshua M. Gorham, Ida G. Lunde, Mingyue Lun, Thomas L. Lynch, James W. McNamara, Sakthivel Sadayappan, Charles S. Redwood, Hugh C. Watkins, Jonathan G. Seidman, and Christine E. Seidman. Hypertrophic cardiomyopathy mutations in MYBPC3 dysregulate myosin. *Science Translational Medicine*, 11(476), jan 2019.

[5] Sabine J. Van Dijk, Dennis Dooijes, Cris Dos Remedios, Michelle Michels, Jos M.J. Lamers, Saul Winegrad, Saskia Schlossarek, Lucie Carrier, Folkert J.Ten Cate, Ger J.M. Stienen, and Jolanda Der Van Velden. Cardiac myosin-binding protein C mutations and hypertrophic ardiomyopathy haploinsufficiency, deranged phosphorylation, and cardiomyocyte dysfunction. *Circulation*, 2009.

[6] Marielle Alders, Roselie Jongbloed, Wout Deelen, Arthur Van den Wijngaard, Pieter Doevendans, Folkert Ten Cate, Vera Regitz-Zagrosek, Hans Peter Vosberg, Irene Van Langen, Arthur Wilde, Dennis Dooijes, and Marcel Mannens. The 2373insG mutation in the MYBPC3 gene is a founder mutation, which accounts for nearly one-fourth of the HCM cases in the Netherlands. *European Heart Journal*, 24(20):1848–1853, oct 2003.

[7] Iman A. Mohamed, Navaneethakrishnan T. Krishnamoorthy, Gheyath K. Nasrallah, and Sahar I. Da'as. The Role of Cardiac Myosin Binding Protein C3 in Hypertrophic Cardiomyopathy-Progress and Novel Therapeutic Opportunities. *Journal of Cellular Physiology*, 232(7):1650–1659, jul 2017.

[8] Adam S. Helms, Vi T. Tang, Thomas S. O'Leary, Sabrina Friedline, Mick Wauchope, Akul Arora, Aaron H. Wasserman, Eric D. Smith, Lap Man Lee, Xiaoquan W. Wen, Jordan A. Shavit, Allen P. Liu, Michael J. Previs, and Sharlene M. Day. Effects of MYBPC3 loss-of-function mutations preceding hypertrophic cardiomyopathy. *JCI Insight*, 5(2), jan 2020.

[9] Adam S. Helms, Francisco J. Alvarado, Jaime Yob, Vi T. Tang, Francis Pagani, Mark W. Russell, Héctor H. Valdivia, and Sharlene M. Day. Genotype-Dependent and -Independent Calcium Signaling Dysregulation in Human Hypertrophic Cardiomyopathy. *Circulation*, 134(22):1738–1748, nov 2016.

[10] James J. Wu, Michael Seco, Caroline Medi, Chris Semsarian, David R. Richmond, Joseph A. Dearani, Hartzell V. Schaff, Michael J. Byrom, and Paul G. Bannon. Surgery for hypertrophic cardiomyopathy. *Biophysical Reviews*, 2015.

[11] Matthew J. Birket, Marcelo C. Ribeiro, Georgios Kosmidis, Dorien Ward, Ana Rita Leitoguinho, Vera van de Pol, Cheryl Dambrot, Harsha D. Devalla, Richard P. Davis, Pier G. Mastroberardino, Douwe E. Atsma, Robert Passier, and Christine L. Mummery. Contractile Defect Caused by Mutation in MYBPC3 Revealed under Conditions Optimized for Human PSC-Cardiomyocyte Function. *Cell Reports*, 13(4):733–745, oct 2015.

[12] Diogo Mosqueira, James G.W. Smith, Jamie R. Bhagwan, and Chris Denning. Modeling Hypertrophic Cardiomyopathy: Mechanistic Insights and Pharmacological Intervention, sep 2019.

[13] Houman Savoji, Mohammad Hossein Mohammadi, Naimeh Rafatian, Masood Khaksar Toroghi, Erika Yan Wang, Yimu Zhao, Anastasia Korolj, Samad Ahadian, and Milica Radisic. Cardiovascular disease models: A game changing paradigm in drug discovery and screening. *Biomaterials*, 198:3–26, apr 2019.

[14] Thierry Vandamme. Use of rodents as models of human diseases, 2014.

[15] Nima Milani-Nejad and Paul M.L. Janssen. Small and large animal models in cardiac contraction research: Advantages and disadvantages, mar 2014.

[16] David Barefield, Mohit Kumar, Joshua Gorham, Jonathan G. Seidman, Christine E. Seidman, Pieter P. de Tombe, and Sakthivel Sadayappan. Haploinsufficiency of MYBPC3 exacerbates the development of hypertrophic cardiomyopathy in heterozygous mice. *Journal of Molecular and Cellular Cardiology*, 79:234–243, feb 2015.

[17] Lutz Pohlmann, Irena Kröger, Nicolas Vignier, Saskia Schlossarek, Elisabeth Krämer, Catherine Coirault, Karim R. Sultan, Ali El-Armouche, Saul Winegrad, Thomas Eschenhagen, and Lucie Carrier. Cardiac myosin-binding protein C is required for complete relaxation in intact myocytes. *Circulation Research*, 101(9):928–938, oct 2007.

[18] Paul J.M. Wijnker, Felix W. Friedrich, Alexander Dutsch, Silke Reischmann, Alexandra Eder, Ingra Mannhardt, Giulia Mearini, Thomas Eschenhagen, Jolanda van der Velden, and Lucie Carrier. Comparison of the effects of a truncating and a missense MYBPC3 mutation on contractile parameters of engineered heart tissue. *Journal of Molecular and Cellular Cardiology*, 97:82–92, aug 2016.

[19] Advantages and Disadvantages of Using Primary Cells in Cell Culture - Kosheeka.

[20] William E. Louch, Katherine A. Sheehan, and Beata M. Wolska. Methods in cardiomyocyte isolation, culture, and gene transfer, sep 2011.

[21] Primary Culture - an overview — ScienceDirect Topics.

[22] William C. Claycomb, Nicholas A. Lanson, Beverly S. Stallworth, Daniel B. Egeland, Joseph B. Delcarpio, Anthony Bahinski, and Nicholas J. Izzo. HL-1 cells: A cardiac muscle cell line that contracts and retains phenotypic characteristics of the adult cardiomyocyte. *Proceedings of the National Academy of Sciences of the United States of America*, 95(6):2979–2984, mar 1998.

[23] B. W. Kimes and B. L. Brandt. Properties of a clonal muscle cell line from rat heart. *Experimental Cell Research*, 98(2):367–381, mar 1976.

[24] Andrey V. Kuznetsov, Sabzali Javadov, Stephan Sickinger, Sandra Frotschnig, and Michael Grimm. H9c2 and HL-1 cells demonstrate distinct features of energy metabolism, mitochondrial function and sensitivity to hypoxia-reoxygenation. *Biochimica et Biophysica Acta - Molecular Cell Research*, 1853(2):276–284, feb 2015.

[25] Xiaowen Bai. Stem Cell-Based Disease Modeling and Cell Therapy, sep 2020.

[26] Michaela Prochazkova, Miquella G. Chavez, Jan Prochazka, Hady Felfy, Vagan Mushegyan, and Ophir D. Klein. Embryonic Versus Adult Stem Cells. In *Stem Cell Biology and Tissue Engineering in Dental Sciences*, pages 249–262. Elsevier Inc., jan 2015.

[27] Kazutoshi Takahashi, Koji Tanabe, Mari Ohnuki, Megumi Narita, Tomoko Ichisaka, Kiichiro Tomoda, and Shinya Yamanaka. Induction of Pluripotent Stem Cells from Adult Human Fibroblasts by Defined Factors. *Cell*, 131(5):861–872, nov 2007.

[28] Kazutoshi Takahashi and Shinya Yamanaka. Induction of Pluripotent Stem Cells from Mouse Embryonic and Adult Fibroblast Cultures by Defined Factors. *Cell*, 126(4):663–676, aug 2006.

[29] Evangeline Tzatzalos, Oscar J. Abilez, Praveen Shukla, and Joseph C. Wu. Engineered heart tissues and induced pluripotent stem cells: Macro- and microstructures for disease modeling, drug screening, and translational studies, jan 2016.

[30] Maksymilian Prondzynski, Elisabeth Krämer, Sandra D. Laufer, Aya Shibamiya, Ole Pless, Frederik Flenner, Oliver J. Müller, Julia Münch, Charles Redwood, Arne Hansen, Monica Patten, Thomas Eschenhagen, Giulia Mearini, and Lucie Carrier. Evaluation of MYBPC3 trans-Splicing and Gene Replacement as Therapeutic Options in Human iPSC-Derived Cardiomyocytes. *Molecular Therapy - Nucleic Acids*, 7:475–486, jun 2017.

[31] Shiv Kumar Viswanathan, Megan J. Puckelwartz, Ashish Mehta, Chrishan J.A. Ramachandra, Aravindakshan Jagadeesan, Regina Fritsche-Danielson, Ratan V. Bhat, Philip Wong, Sangeetha Kandoi, Jennifer A. Schwanekamp, Gina Kuffel, Lorenzo L. Pesce, Michael J. Zilliox, U. Nalla B. Durai, Rama Shanker Verma, Robert E. Molokie, Domodhar P. Suresh, Philip R. Khoury, Annie Thomas, Thriveni Sanagala, Hak Chiaw Tang, Richard C. Becker, Ralph Knoll, Winston Shim, Elizabeth M. McNally, and Sakthivel Sadayappan. Association of cardiomyopathy with MYBPC3 D389V and MYBPC3 Δ25bp intronic deletion in south asian descendants. *JAMA Cardiology*, 3(6):481–488, jun 2018.

[32] Yee Ki Lee, X. Ran, K. W.H. Lai, V. Y.M. Lau, D. C.W. Siu, and H. F. Tse. Generation and characterization of patient-specific iPSC model for cardiovascular disease. In *Methods in Molecular Biology*, volume 1353, pages 191–213. Humana Press Inc., 2016.

[33] Claudia Sacchetto, Libero Vitiello, Leon J. de Windt, Alessandra Rampazzo, and Martina Calore. Modeling cardiovascular diseases with hipsc-derived cardiomyocytes in 2d and 3d cultures, may 2020.

[34] Chun Liu, Angelos Oikonomopoulos, Nazish Sayed, and Joseph C. Wu. Modeling human diseases with induced pluripotent stem cells: From 2D to 3D and beyond. *Development (Cambridge)*, 145(5), mar 2018.

[35] Cassady E. Rupert, Tae Yun Kim, Bum Rak Choi, and Kareen L.K. Coulombe. Human Cardiac Fibroblast Number and Activation State Modulate Electromechanical Function of hiPSC-Cardiomyocytes in Engineered Myocardium. *Stem Cells International*, 2020, 2020.

[36] Cheryl Dambrot, Stefan R. Braam, Leon G.J. Tertoolen, Matthew Birket, Douwe E. Atsma, and Christine L. Mummery. Serum supplemented culture medium masks hypertrophic phenotypes in human pluripotent stem cell derived cardiomyocytes. *Journal of Cellular and Molecular Medicine*, 18(8):1509–1518, 2014.

[37] Verena Schwach and Robert Passier. Generation and purification of human stem cell-derived cardiomyocytes, apr 2016.

[38] Maya Fuerstenau-Sharp, Martina E. Zimmermann, Klaus Stark, Nico Jentsch, Melanie Klingenstein, Marzena Drzymalski, Stefan Wagner, Lars S. Maier, Ute Hehr, Andrea Baessler, Marcus Fischer, and Christian Hengstenberg. Generation of highly purified human cardiomyocytes from peripheral blood mononuclear cell-derived induced pluripotent stem cells. *PLoS ONE*, 2015.

[39] Kiwon Ban, Seongho Bae, and Young sup Yoon. Current strategies and challenges for purification of cardiomyocytes derived from human pluripotent stem cells, 2017.

[40] Cassady E. Rupert, Chinedu Irofuala, and Kareen L.K. Coulombe. Practical adoption of state-of-the-art hiPSC-cardiomyocyte differentiation techniques. *PLoS ONE*, 15(3), 2020.

[41] Shugo Tohyama and Keiichi Fukuda. Future treatment of heart failure using human iPSC-derived cardiomyocytes. In *Etiology and Morphogenesis of Congenital Heart Disease: From Gene Function and Cellular Interaction to Morphology*, pages 25–31. Springer Japan, jan 2016.

[42] Shugo Tohyama, Fumiyuki Hattori, Motoaki Sano, Takako Hishiki, Yoshiko Nagahata, Tomomi Matsuura, Hisayuki Hashimoto, Tomoyuki Suzuki, Hiromi Yamashita, Yusuke Satoh, Toru Egashira, Tomohisa Seki, Naoto Muraoka, Hiroyuki Yamakawa, Yasuyuki Ohgino, Tomofumi Tanaka, Masatoshi Yoichi, Shinsuke Yuasa, Mitsushige Murata, Makoto Suematsu, and Keiichi Fukuda. Distinct metabolic flow enables large-scale purification of mouse and human pluripotent stem cell-derived cardiomyocytes. *Cell Stem Cell*, 12(1):127–137, jan 2013.

[43] Claudia De Masi, Paola Spitalieri, Michela Murdocca, Giuseppe Novelli, and Federica Sangiuolo. Application of CRISPR/Cas9 to human-induced pluripotent stem cells: From gene editing to drug discovery, jun 2020.

[44] Přemysl Mladěnka, Lenka Applová, Jiří Patočka, Vera Marisa Costa, Fernando Remiao, Jana Pourová, Aleš Mladěnka, Jana Karlíčková, Luděk Jahodář, Marie Vopršalová, Kurt J. Varner, and Martin Štěrba. Comprehensive review of cardiovascular toxicity of drugs and related agents, 2018.

[45] What are genome editing and CRISPR-Cas9?: MedlinePlus Genetics.

[46] CRISPR-Cas9: The Gene Editing Tool Changing the World.

[47] Thomas Eschenhagen, Christine Fink, Ute Remmers, Hasso Scholz, Jens Wattchow, Joachim Weil, Wolfram Zimmermann, Hans H. Dohmen, Hansjörg Schäfer, Nanette Bishopric, Tetsuro Wakatsuki, and Elliot L. Elson. Three-dimensional reconstitution of embryonic cardiomyocytes in a collagen matrix: a new heart muscle model system. *The FASEB Journal*, 11(8):683–694, jul 1997.

[48] W. H. Zimmermann, K. Schneiderbanger, P. Schubert, M. Didié, F. Münzel, J. F. Heubach, S. Kostin, W. L. Neuhuber, and T. Eschenhagen. Tissue engineering of a differentiated cardiac muscle construct. *Circulation Research*, 90(2):223–230, feb 2002.

[49] Arne Hansen, Alexandra Eder, Marlene Bönstrup, Marianne Flato, Marco Mewe, Sebastian Schaaf, Bülent Aksehirlioglu, Alexander Schwörer, June Uebeler, and Thomas Eschenhagen. Development of a drug screening platform based on engineered heart tissue. *Circulation Research*, 107(1):35–44, jul 2010.

[50] Sebastian Schaaf, Aya Shibamiya, Marco Mewe, Alexandra Eder, Andrea Stöhr, Marc N. Hirt, Thomas Rau, Wolfram Hubertus Zimmermann, Lenard Conradi, Thomas Eschenhagen, and Arne Hansen. Human engineered heart tissue as a versatile tool in basic research and preclinical toxicology. *PLoS ONE*, 2011.

[51] Kaja Breckwoldt, David Letuffe-Brenière, Ingra Mannhardt, Thomas Schulze, Bärbel Ulmer, Tessa Werner, Anika Benzin, Birgit Klampe, Marina C. Reinsch, Sandra Laufer, Aya Shibamiya, Maksymilian Prondzynski, Giulia Mearini, Dennis Schade, Sigrid Fuchs, Christiane Neuber, Elisabeth Krämer, Umber Saleem, Mirja L. Schulze, Marita L. Rodriguez, Thomas Eschenhagen, and Arne Hansen. Differentiation of cardiomyocytes and generation of human engineered heart tissue. *Nature Protocols*, 2017.

[52] Marc N. Hirt, Nils A. Sörensen, Lena M. Bartholdt, Jasper Boeddinghaus, Sebastian Schaaf, Alexandra Eder, Ingra Vollert, Andrea Stöhr, Thomas Schulze, Anika Witten, Monika Stoll, Arne Hansen, and Thomas Eschenhagen. Increased afterload induces pathological cardiac hypertrophy: a new in vitro model. *Basic Research in Cardiology*, 107(6):307, nov 2012.

[53] Marc D. Lemoine, Ingra Mannhardt, Kaja Breckwoldt, Maksymilian Prondzynski, Frederik Flenner, Bärbel Ulmer, Marc N. Hirt, Christiane Neuber, András Horváth, Benjamin Kloth, Hermann Reichenspurner, Stephan Willems, Arne Hansen, Thomas Eschenhagen, and Torsten Christ. Human iPSC-derived cardiomyocytes cultured in 3D engineered heart tissue show physiological upstroke velocity and sodium current density. *Scientific Reports*, 7(1), dec 2017.

[54] Kacey Ronaldson-Bouchard, Stephen P. Ma, Keith Yeager, Timothy Chen, Lou Jin Song, Dario Sirabella, Kumi Morikawa, Diogo Teles, Masayuki Yazawa, and Gordana Vunjak-Novakovic. Advanced maturation of human cardiac tissue grown from pluripotent stem cells. *Nature*, 2018.

[55] Marta Lemme, Bärbel M. Ulmer, Marc D. Lemoine, Antonia T.L. Zech, Frederik Flenner, Ursula Ravens, Hermann Reichenspurner, Miriam Rol-Garcia, Godfrey Smith, Arne Hansen, Torsten Christ, and Thomas Eschenhagen. Atrial-like Engineered Heart Tissue: An In Vitro Model of the Human Atrium. *Stem Cell Reports*, 11(6):1378–1390, dec 2018.

[56] Idit Goldfracht, Yael Efraim, Rami Shinnawi, Ekaterina Kovalev, Irit Huber, Amira Gepstein, Gil Arbel, Naim Shaheen, Malte Tiburcy, Wolfram H. Zimmermann, Marcelle Machluf, and Lior Gepstein. Engineered heart tissue models from hiPSC-derived cardiomyocytes and cardiac ECM for disease modeling and drug testing applications. *Acta Biomaterialia*, 92:145–159, jul 2019.

[57] Idit Goldfracht, Stephanie Protze, Assad Shiti, Noga Setter, Amit Gruber, Naim Shaheen, Yulia Nartiss, Gordon Keller, and Lior Gepstein. Generating ring-shaped engineered heart tissues from ventricular and atrial human pluripotent stem cell-derived cardiomyocytes. *Nature Communications*, 11(1):1–15, dec 2020.

[58] Diogo Mosqueira, Ingra Mannhardt, Jamie R. Bhagwan, Katarzyna Lis-Slimak, Puspita Katili, Elizabeth Scott, Mustafa Hassan, Maksymilian Prondzynski, Stephen C. Harmer, Andrew Tinker, James G.W. Smith, Lucie Carrier, Philip M. Williams, Daniel Gaffney, Thomas Eschenhagen, Arne Hansen, and Chris Denning. CRISPR/Cas9 editing in human pluripotent stemcell-cardiomyocytes highlights arrhythmias, hypocontractility, and energy depletion as potential therapeutic targets for hypertrophic cardiomyopathy. *European Heart Journal*, 39(43):3879–3892, nov 2018.

[59] Tadashi Takaki, Azusa Inagaki, Kazuhisa Chonabayashi, Keiji Inoue, Kenji Miki, Seiko Ohno, Takeru Makiyama, Minoru Horie, and Yoshinori Yoshida. Optical recording of action potentials in human induced pluripotent stem cell-derived cardiac single cells and monolayers generated from long QT syndrome type 1 patients. *Stem Cells International*, 2019, 2019.

[60] Christian Zuppinger. 3D Cardiac Cell Culture: A Critical Review of Current Technologies and Applications, jun 2019.

[61] John T. Hinson, Anant Chopra, Navid Nafissi, William J. Polacheck, Craig C. Benson, Sandra Swist, Joshua Gorham, Luhan Yang, Sebastian Schafer, Calvin C. Sheng, Alireza Haghighi, Jason Homsy, Norbert Hubner, George Church, Stuart A. Cook, Wolfgang A. Linke, Christopher S. Chen, J. G. Seidman, and Christine E. Seidman. Titin mutations in iPS cells define sarcomere insufficiency as a cause of dilated cardiomyopathy. *Science*, 349(6251):982–986, aug 2015.

[62] Huaxiao Yang, Ningyi Shao, Alexandra Holmström, Xin Zhao, Tony Chour, Haodong Chen, Ilanit Itzhaki, Haodi Wu, Mohamed Ameen, Nathan J Cunningham, Chengyi Tu, Ming-Tao Zhao, Alice F Tarantal, Oscar J Abilez, and Joseph C Wu. Transcriptome analysis of non human primate-induced pluripotent stem cell-derived cardiomyocytes in 2D monolayer culture vs. 3D engineered heart tissue. *Cardiovascular Research*, oct 2020.

[63] Charan Thej, Grace Huang, and Raj Kishore. Three-dimensional unity of engineered heart tissue mimics the heart better than two-dimensional cellular diversity. *Cardiovascular Research*, feb 2021.

[64] Ingra Vollert, Moritz Seiffert, Johanna Bachmair, Merle Sander, Alexandra Eder, Lenard Conradi, Alexander Vogelsang, Thomas Schulze, June Uebeler, Wolfgang Holnthoner, Heinz Redl, Hermann Reichenspurner, Arne Hansen, and Thomas Eschenhagen. In vitro perfusion of engineered heart tissue through endothelialized channels. *Tissue Engineering - Part A*, 20(3-4):854–863, feb 2014.

[65] Tomasz Jan Kolanowski, Mathias Busek, Mario Schubert, Anna Dmitrieva, Björn Binneweg, Jessie Pöche, Konstanze Fisher, Florian Schmieder, Stefan Grünzner, Sinah Hansen, Andreas Richter, Ali El-Armouche, Frank Sonntag, and Kaomei Guan. Enhanced structural maturation of human induced pluripotent stem cell-derived cardiomyocytes under a controlled microenvironment in a microfluidic system. *Acta Biomaterialia*, 102:273–286, jan 2020.

[66] Lai Wei, Weizhen Li, Emilia Entcheva, and Zhenyu Li. Microfluidics-enabled 96-well perfusion system for high-throughput tissue engineering and long-term all-optical electrophysiology. *Lab on a Chip*, 20(21):4031–4042, nov 2020.

[67] Bärbel M. Ulmer and Thomas Eschenhagen. Human pluripotent stem cell-derived cardiomyocytes for studying energy metabolism, mar 2020.

[68] Christopher P. Jackman, Aaron L. Carlson, and Nenad Bursac. Dynamic culture yields engineered myocardium with near-adult functional output. *Biomaterials*, 111:66–79, dec 2016.

[69] Ling Gao, Zachery R. Gregorich, Wuqiang Zhu, Saidulu Mattapally, Yasin Oduk, Xi Lou, Ramaswamy Kannappan, Anton V. Borovjagin, Gregory P. Walcott, Andrew E. Pollard, Vladimir G. Fast, Xinyang Hu, Steven G. Lloyd, Ying Ge, and Jianyi Zhang. Large cardiac

muscle patches engineered from human induced-pluripotent stem cell-derived cardiac cells improve recovery from myocardial infarction in swine. *Circulation*, 137(16):1712–1730, 2018.

[70] Celinda M. Kofron and Ulrike Mende. In vitro models of the cardiac microenvironment to study myocyte and non-myocyte crosstalk: bioinspired approaches beyond the polystyrene dish, jun 2017.

[71] Dimitry A. Chistiakov, Alexander N. Orekhov, and Yuri V. Bobryshev. The role of cardiac fibroblasts in post-myocardial heart tissue repair, oct 2016.

[72] Virpi Talman and Riikka Kivelä. Cardiomyocyte—Endothelial Cell Interactions in Cardiac Remodeling and Regeneration, jul 2018.

[73] Andrea Colliva, Luca Braga, Mauro Giacca, and Serena Zacchigna. Endothelial cell–cardiomyocyte crosstalk in heart development and disease. *The Journal of Physiology*, 598(14):2923–2939, jul 2020.

[74] Harpinder Saini, Ali Navaei, Alison Van Putten, and Mehdi Nikkhah. 3D Cardiac Microtissues Encapsulated with the Co-Culture of Cardiomyocytes and Cardiac Fibroblasts. *Advanced Healthcare Materials*, 4(13):1961–1971, sep 2015.

[75] Elisa Giacomelli, Viviana Meraviglia, Giulia Campostrini, Amy Cochrane, Xu Cao, Ruben W.J. van Helden, Ana Krotenberg Garcia, Maria Mircea, Sarantos Kostidis, Richard P. Davis, Berend J. van Meer, Carolina R. Jost, Abraham J. Koster, Hailiang Mei, David G. Míguez, Aat A. Mulder, Mario Ledesma-Terrón, Giulio Pompilio, Luca Sala, Daniela C.F. Salvatori, Roderick C. Slieker, Elena Sommariva, Antoine A.F. de Vries, Martin Giera, Stefan Semrau, Leon G.J. Tertoolen, Valeria V. Orlova, Milena Bellin, and Christine L. Mummery. Human-iPSC-Derived Cardiac Stromal Cells Enhance Maturation in 3D Cardiac Microtissues and Reveal Non-cardiomyocyte Contributions to Heart Disease. *Cell Stem Cell*, 26(6):862–879.e11, jun 2020.

[76] David E. Procaccini, Jaclyn E. Sawyer, and Kevin M. Watt. Pharmacology of cardiovascular drugs. In *Critical Heart Disease in Infants and Children*, pages 192–212.e6. Elsevier, jan 2018.

[77] Maxime Cannesson, Zhongping Jian, Guo Chen, Trung Q. Vu, and Feras Hatib. Effects of phenylephrine on cardiac output and venous return depend on the position of the heart on the Frank-Starling relationship. *Journal of Applied Physiology*, 113(2):281–289, jul 2012.

[78] Liem P. Nguyen and Neal S. Gerstein. Cardiovascular pharmacology in noncardiac surgery. In *Essentials of Cardiac Anesthesia for Noncardiac Surgery: A Companion to Kaplan's Cardiac Anesthesia*, pages 247–288. Elsevier, jan 2018.

[79] Gábor Földes, Maxime Mioulane, Jamie S. Wright, Alexander Q. Liu, Pavel Novak, Béla Merkely, Julia Gorelik, Michael D. Schneider, Nadire N. Ali, and Sian E. Harding. Modulation of human embryonic stem cell-derived cardiomyocyte growth: A testbed for studying human cardiac hypertrophy? *Journal of Molecular and Cellular Cardiology*, 2011.

[80] Chang Peng, Xiaomei Luo, Shuo Li, and Huichao Sun. Phenylephrine-induced cardiac hypertrophy is attenuated by a histone acetylase inhibitor anacardic acid in mice. *Molecular BioSystems*, 13(4):714–724, mar 2017.

[81] Cassady E. Rupert, Heidi H. Chang, and Kareen L.K. Coulombe. Hypertrophy Changes 3D Shape of hiPSC-Cardiomyocytes: Implications for Cellular Maturation in Regenerative Medicine. *Cellular and Molecular Bioengineering*, 10(1):54–62, feb 2017.

[82] Thomas Eschenhagen, Christine Mummery, and Bjorn C. Knollmann. Modelling sarcomeric cardiomyopathies in the dish: From human heart samples to iPSC cardiomyocytes, apr 2015.

[83] Zhen Ma, Nathaniel Huebsch, Sangmo Koo, Mohammad A. Mandegar, Brian Siemons, Steven Boggess, Bruce R. Conklin, Costas P. Grigoropoulos, and Kevin E. Healy. Contractile deficits in engineered cardiac microtissues as a result of MYBPC3 deficiency and mechanical overload. *Nature Biomedical Engineering*, 2(12):955–967, dec 2018.

[84] Milena Bellin, Simona Casini, Richard P. Davis, Cristina D'Aniello, Jessica Haas, Dorien Ward-Van Oostwaard, Leon G.J. Tertoolen, Christian B. Jung, David A. Elliott, Andrea Welling, Karl Ludwig Laugwitz, Alessandra Moretti, and Christine L. Mummery. Isogenic human pluripotent stem cell pairs reveal the role of a KCNH2 mutation in long-QT syndrome. *EMBO Journal*, 32(24):3161–3175, dec 2013.

[85] Verena Schwach, Arie O. Verkerk, Mervyn Mol, Jantine J. Monshouwer-Kloots, Harsha D. Devalla, Valeria V. Orlova, Konstantinos Anastassiadis, Christine L. Mummery, Richard P. Davis, and Robert Passier. A COUP-TFII Human Embryonic Stem Cell Reporter Line to Identify and Select Atrial Cardiomyocytes. *Stem Cell Reports*, 9(6):1765–1779, dec 2017.

[86] Kaitlin K. Dunn, Isabella M. Reichardt, Aaron D. Simmons, Gyuhyung Jin, Martha E. Floy, Kelsey M. Hoon, and Sean P. Palecek. Coculture of Endothelial Cells with Human Pluripotent Stem Cell-Derived Cardiac Progenitors Reveals a Differentiation Stage-Specific Enhancement of Cardiomyocyte Maturation. *Biotechnology Journal*, 14(8):e1800725, aug 2019.

[87] David Barefield, Mohit Kumar, Pieter P. de Tombe, and Sakthivel Sadayappan. Contractile dysfunction in a mouse model expressing a heterozygous MYBPC3 mutation associated with hypertrophic cardiomyopathy. *American Journal of Physiology - Heart and Circulatory Physiology*, 306(6):807–815, mar 2014.

[88] Andrea Stoehr, Christiane Neuber, Christina Baldauf, Ingra Vollert, Felix W. Friedrich, Frederik Flenner, Lucie Carrier, Alexandra Eder, Sebastian Schaaf, Marc N. Hirt, Bülent Aksehirlioglu, Carl W. Tong, Alessandra Moretti, Thomas Eschenhagen, and Arne Hansen. Automated analysis of contractile force and Ca2+ transients in engineered heart tissue. *American Journal of Physiology - Heart and Circulatory Physiology*, 306(9):H1353, may 2014.

[89] Marisa Ojala, Chandra Prajapati, Risto Pekka Pölönen, Kristiina Rajala, Mari Pekkanen-Mattila, Jyrki Rasku, Kim Larsson, and Katriina Aalto-Setälä. Mutation-specific phenotypes in hiPSC-derived cardiomyocytes carrying either myosin-binding protein C or α -tropomyosin mutation for hypertrophic cardiomyopathy. *Stem Cells International*, 2016, 2016.

[90] Saowanee Jiwlawat, Eileen Lynch, Jennifer Glaser, Ivy Smit-Oistad, Jeremy Jeffrey, Jonathan M. Van Dyke, and Masatoshi Suzuki. Differentiation and sarcomere formation in skeletal myocytes directly prepared from human induced pluripotent stem cells using a sphere-based culture. *Differentiation*, 96:70–81, jul 2017.

[91] Hiroshi Naito, Ivan Melnychenko, Michael Didié, Karin Schneiderbanger, Pia Schubert, Stephan Rosenkranz, Thomas Eschenhagen, and Wolfram Hubertus Zimmermann. Optimizing engineered heart tissue for therapeutic applications as surrogate heart muscle. *Circulation*, 114(SUPPL. 1), jul 2006.

[92] Gabor Földes, Elena Matsa, János Kriston-Vizi, Thomas Leja, Stefan Amisten, Ljudmila Kolker, Thusharika Kodagoda, Nazanin F. Dolatshad, Maxime Mioulane, Karine Vauchez, Tamás Arányi, Robin Ketteler, Michael D. Schneider, Chris Denning, and Sian E. Harding. Aberrant α-adrenergic hypertrophic response in Cardiomyocytes from human induced pluripotent cells. *Stem Cell Reports*, 3(5):905–914, 2014.

[93] Justus Stenzig, Marc N. Hirt, Alexandra Löser, Lena M. Bartholdt, Jan Tobias Hensel, Tessa R. Werner, Mona Riemenschneider, Daniela Indenbirken, Thomas Guenther, Christian Müller, Norbert Hübner, Monika Stoll, and Thomas Eschenhagen. DNA methylation in an engineered heart tissue model of cardiac hypertrophy: common signatures and effects of DNA methylation inhibitors. *Basic Research in Cardiology*, 111(1):1–14, jan 2016.

[94] Felix W. Friedrich, Silke Reischmann, Aileen Schwalm, Andreas Unger, Deepak Ramanujam, Julia Münch, Oliver J. Müller, Christian Hengstenberg, Enrique Galve, Philippe Charron, Wolfgang A. Linke, Stefan Engelhardt, Monica Patten, Pascale Richard, Jolanda van der Velden, Thomas Eschenhagen, Richard Isnard, and Lucie Carrier. FHL2 expression and variants in hypertrophic cardiomyopathy. *Basic Research in Cardiology*, 109(6):451, nov 2014.

[95] Linlin Shang, Lv Pin, Shanshan Zhu, Xiaohang Zhong, Yubiao Zhang, Mao Shun, Yunen Liu, and Mingxiao Hou. Plantamajoside attenuates isoproterenol-induced cardiac hypertrophy associated with the HDAC2 and AKT/ GSK-3β signaling pathway. *Chemico-Biological Interactions*, 307:21–28, jul 2019.

[96] Yu Shrike Zhang, Andrea Arneri, Simone Bersini, Su Ryon Shin, Kai Zhu, Zahra Goli-Malekabadi, Julio Aleman, Cristina Colosi, Fabio Busignani, Valeria Dell'Erba, Colin Bishop, Thomas Shupe, Danilo Demarchi, Matteo Moretti, Marco Rasponi, Mehmet Remzi Dokmeci, Anthony Atala, and Ali Khademhosseini. Bioprinting 3D microfibrous scaffolds for engineering endothelialized myocardium and heart-on-a-chip. *Biomaterials*, 110:45–59, dec 2016.

[97] Xuetao Sun, Wafa Altalhi, and Sara S. Nunes. Vascularization strategies of engineered tissues and their application in cardiac regeneration, jan 2016.

Supplement A. Basic CM medium

Component	Final Concentration	For 1 liter
DMEM	111 mM Na	8.3 gr
Sodium Pyruvate	0.5 mM	5 ml
Sodium 3-hydroxybutyrate	0.19 mM	0.024 gr
L-Carnitine hydrochloride	0.5 mM	0.1 gr
Creatine monohydrate	1 mM	0.15 gr
Taurine	5 mM	0.626 gr
Phenol Red		0.011 gr
Distilled Water		961 ml
Trace elements A	1x	1 ml
Trace elements B	1x	1 ml
Trace elements C	1x	1 ml
Chemically defined lipid concentrate	1x	10 ml
GlutaMAX Supplement	1x	10 ml
1-Thioglycerol (α-MTG)	0.45 mM	39 µl (of undiluted stock)
Insulin-Transferrin-Selenium Ethanolamine (ITS-X)	0.01x	100 µl
Ascorbic acid-2P	50 µg/ml	10 ml
Penicillin-Streptomycin	0.5x	5 ml
Sodium hydrogen carbonate ($NaHCO_3$)	35.7 mM Na to bring final [Na] of 148 mM	3.7 gr

Supplement B. Chip seeding (made by Tom Boonen)

Equipment

Chips	Counting chamber	Fibrinogen (20mg/mL)
Cells	tryplE select	Matrigel (100uL/mL)
Pluronic-F127 (1% in H2O)	Centrifuge	2x CM medium
LAF cabinet with microscope	DPBS	

Methods/procedures

1. Pluronic treatment

1. Pipet Pluronic-F127 into the top channel, filling all the EHT chambers but not the bottom channel. (Figure 1B)
2. Incubate at RT for >20min.
3. Flush from the bottom channel with PBS so that no Pluronic enters the bottom channels.
4. Aspirate the PBS until the chips is **completely dry!** This can be done before starting work on the cells.

2. Cell dissociation

1. Aspirate medium from the cells.
2. Wash the cells with 2mL/well of DPBS.
3. Add 1mL/well tryplE select and incubate at 37C for 10min.
4. Per 1mL of tryplE add 3mL MEF medium to a 15mL tube.
5. Dissociate the cells and add them to the tube.
6. Flush the well with 1mL of MEF.
7. Centrifuge the tube at 1100rpm for 3min.
8. Aspirate excess medium and resuspend in 1mL CM.
9. Count cells and resuspend in the desired volume (usually 20mln/mL)

3. Gel-cell mixture

1. Put an aliquot of Matrigel and Fibrinogen on ice.
2. Of the total volume you want to make, add 10% Fibrinogen, 10% 2xCM, 10% Matrigel, 70% Cell suspension to an Eppendorf.
3. Have the chip ready under the microscope, together with a p200 with tip to resuspend and seed.
4. Add thrombin to the gel-cell mixture (0.3% of total volume).
5. Resuspend the mixture and seed the mixture into the top channel, filling the EHT chamber until the bottom resistance (Figure 1C).
6. Take up the mixture from the top channel and let the gel polymerize for 10min (Figure 1D).
7. Add medium (CM +TI +HS??) to the top and bottom channel and add pipet tips (p200) with medium. A very small volume of medium on the outlets on the right side and 200µL in the tips in the inlets on the left side. The medium will start to equilibrate immediately.

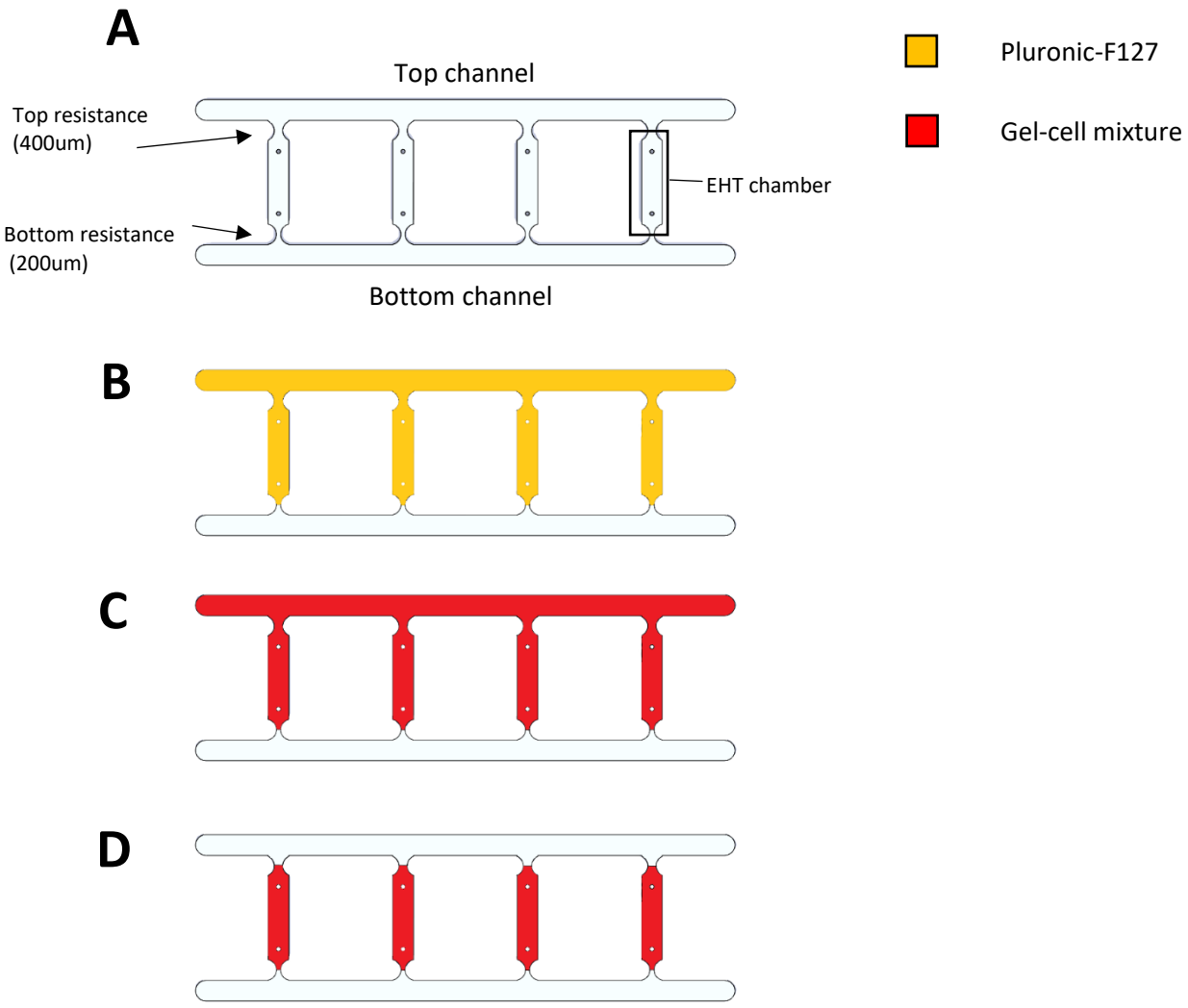

Figure 1: A| All terminology used for the chip parts. **B|** After hydrophobic recovery chips are treated with Pluronic-F127 up until the bottom resistance. **C|** Cell are seeded through the top channel up until the bottom channel. **D|** Top cells in the top channel are taken up again with the pipet, leaving only the EHT chambers filled with cells.

9 Supplementary figures

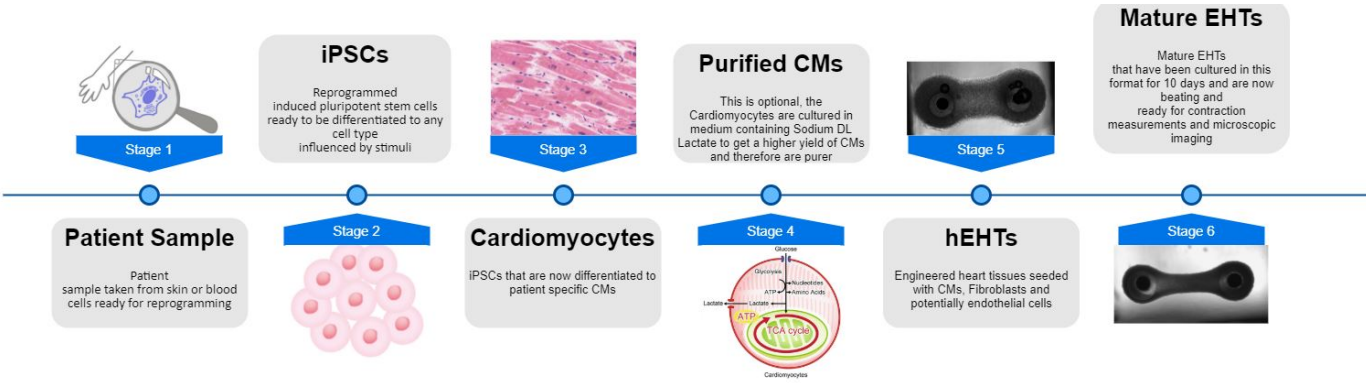

Figure S1: Timeline of the hIPSCs until the moment of measurement of the engineered heart tissues, it gives a visual representation of the formation timeline of the EHTs. From the moment of the biopsy that is taken from the patient towards the matured engineered heart tissue that can be used to do contraction measurements and microscopic imaging to assess the contractility of the used cells. As can be seen in the figure, the maturation of the EHTs takes around 10 days, which is the day that the measurements can be carried out.

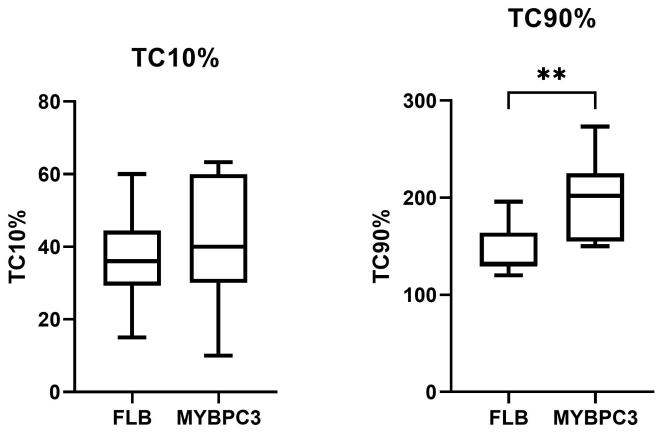

Figure S2: The TC10% and TC90% of the FLB and MYBPC3 cell lines ** $p<0.01$ generated in the FHCM model using un-purified CMs

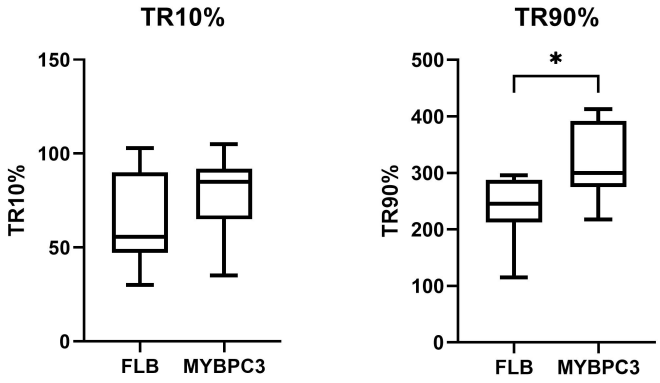

Figure S3: The TR10% and TR90% of the FLB and MYBPC3 cell lines * $p<0.05$ generated in the FHCM model using un-purified CMs

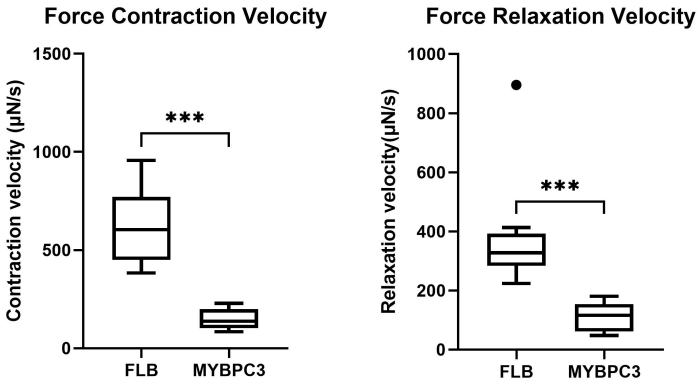

Figure S4: The force contraction and relaxation velocities generated in the FHCM model using un-purified CMs *** $p<0.001$

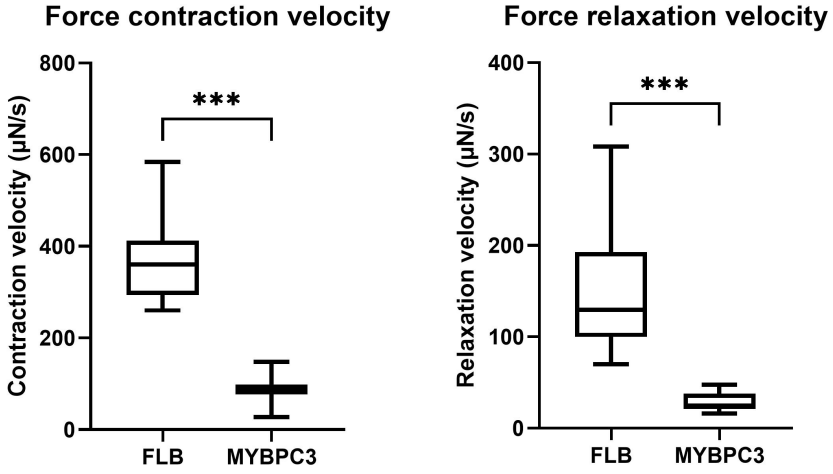

Figure S5: The force contraction and relaxation velocities of the FLB and MYBPC3 cell lines *** $P<0.001$ generated in the FHCM model using lactate purified CMs

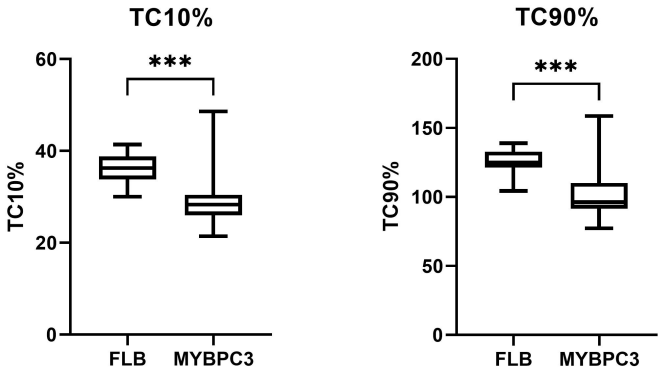

Figure S6: TC10% and TC90% of the FLB and MYBPC3 cells *** $p<0.001$ generated in the FHCM model using lactate purifed CMs

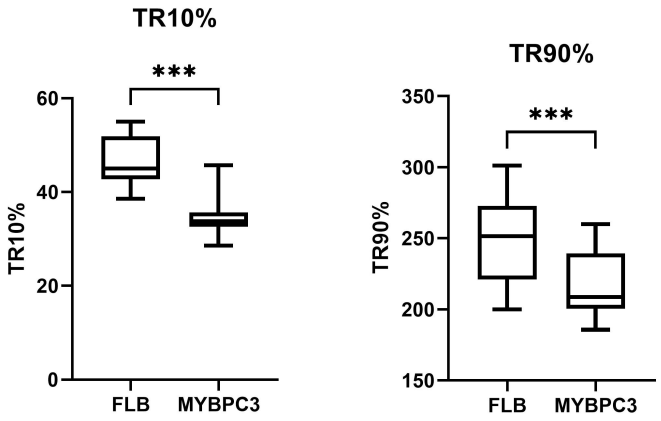

Figure S7: TR10% and TR90% of the FLB and MYBPC3 cells *** $p<0.001$ generated in the FHCM model using lactate purifed CMs

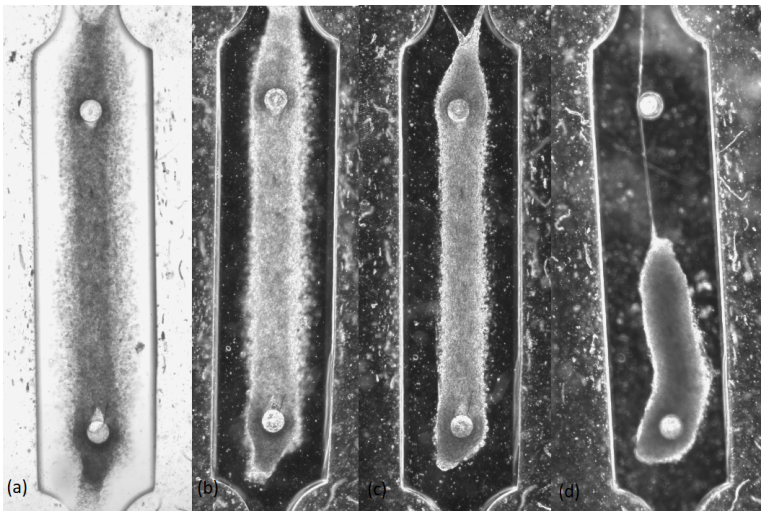

Figure S8: Formation of the microEHTs using only CMs (a)d1 (b)d2 (c)d3 (d)d6. strings of CMs that cling to the top of the chip are still an issue here

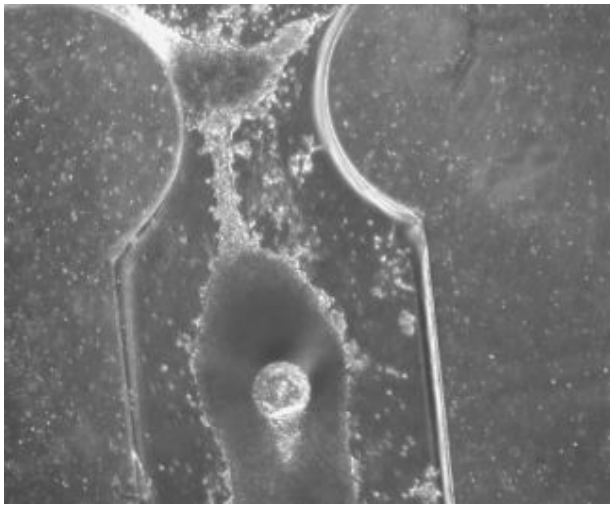

Figure S9: Picture of the chamber entrance of to the top channel of the chip, the clot in the top blocks off this entrance, disrupting the medium flow to the chamber

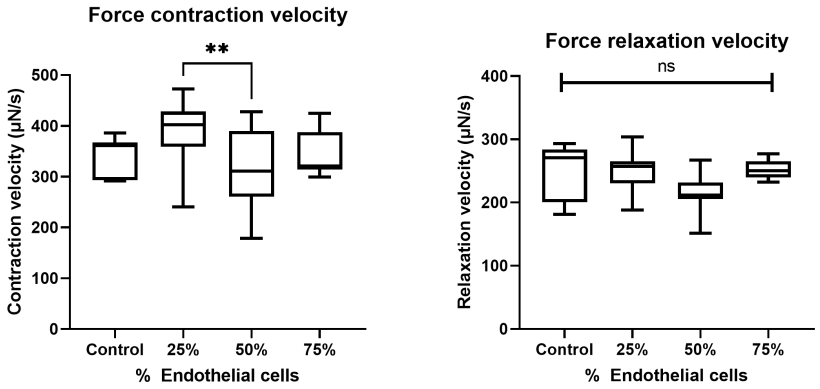

Figure S10: The force contraction and relaxation velocities of the tissues with different percentages of ECs ** $p<0.01$

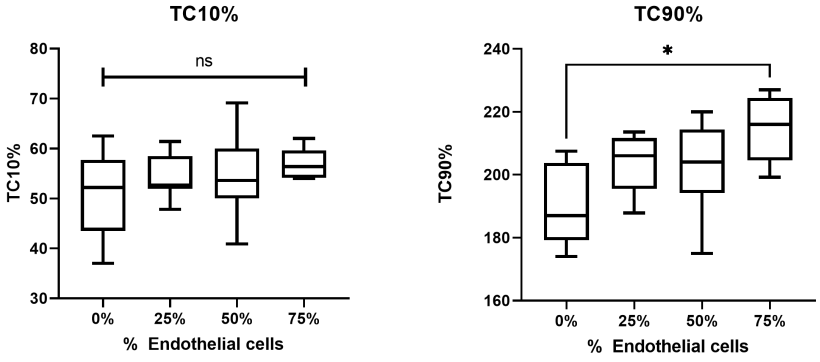

Figure S11: TC 10% and TC 90% of the tissues with different percentages of ECs * $p<0.05$

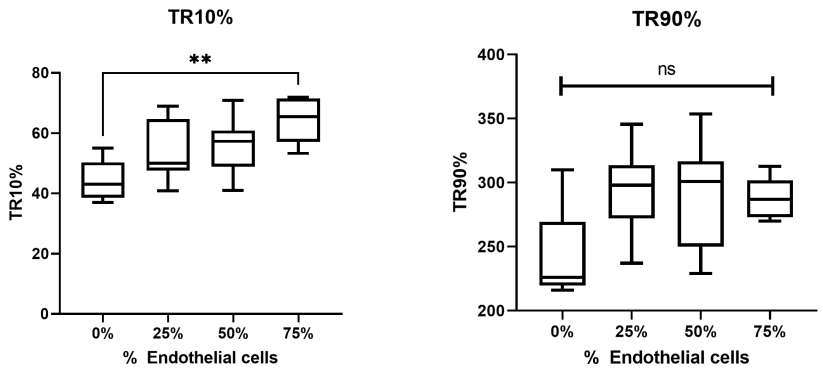

Figure S12: TR 10% and TR 90% of the tissues with different percentages of ECs ** $p<0.001$

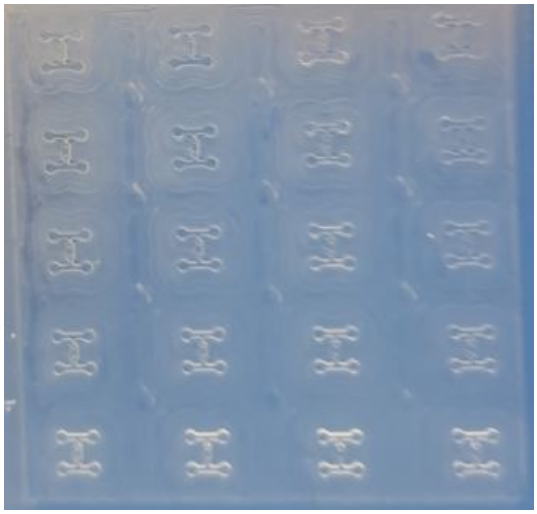

Figure S13: Picture of the nanoEHT mold